

# Periodic Orbit Theory and Spectral Statistics for Quantum Graphs

Tsampikos Kottos and Uzy Smilansky

*Department of Physics of Complex Systems, The Weizmann Institute of Science,  
Rehovot 76100, Israel*

Received November 10, 1998

We quantize graphs (networks) which consist of a finite number of bonds and vertices. We show that the spectral statistics of fully connected graphs is well reproduced by random matrix theory. We also define a classical phase space for the graphs, where the dynamics is mixing and the periodic orbits proliferate exponentially. An exact trace formula for the quantum spectrum is developed in terms of the same periodic orbits, and it is used to investigate the origin of the connection between random matrix theory and the underlying chaotic classical dynamics. Being an exact theory, and due to its relative simplicity, it offers new insights into this problem which is at the forefront of the research in quantum chaos and related fields. © 1999 Academic Press

## I. INTRODUCTION

Quantum graphs (networks) of one-dimensional wires connected at nodes were introduced already more than half a century ago to model physical systems. To the best of our knowledge, they appeared for the first time in connection with free electron models of organic molecules [1–8]. The molecules were visualized as a set of atoms at fixed locations connected by bond paths, along which the electrons obey a one-dimensional Schrödinger equation with an appropriate potential. In recent years the interest in quantum graphs has been revived in many areas of physics, and in particular in the context of condensed matter physics. Among the systems which were successfully modeled by quantum graphs we mention, e.g., studies of superconductivity in granular and artificial materials [9], single-mode acoustic and electromagnetic waveguide networks [10, 11], Anderson transition [12] and quantum Hall systems with long range potential [13], fracton excitations in fractal structures [14], and mesoscopic quantum systems [15]. The construction of the wave equations for such networks is a topic in its own right. Rudenberg and Scherr [4] (see also [8]), who were apparently among the first to address the problem, based their formulation on the analysis of the limit of wires of finite thickness. Quantum graphs can be considered as idealizations of physical networks in the limit where the widths of the wires are much smaller than all the other length scales in the problem. Thus, neglecting the lateral size of the wire, i.e., assuming that the propagating waves remain in a single transverse mode, one replaces the corresponding

partial differential Schrödinger equation by an ordinary differential operator. This can be justified assuming that the inter-mode coupling involves a dynamical tunneling and therefore it diminishes exponentially with the decreasing wire thickness. Moreover, when no external field is applied, the motion on the bonds is free, and the problem can be further reduced to finite matrices [9, 16]. Alexander [9] was probably the first to discuss networks in external magnetic fields.

Quantum graphs attracted the attention of the mathematics community as well. J. P. Roth [17] was probably the first to derive a trace formula for the spectrum of a Laplacian on graphs. Recently the problem came of age in a series of mathematical works by Exner and Seba [18, 19], Avron [16, 20], and Carlson [21], whose formulation is based on the von Neumann theory of self-adjoint extensions of formal differential operators (see also [22] and references therein).

In spite of all this activity, the statistical properties of the spectra displayed by quantum graphs were hardly investigated in the past [13, 23]. Our motivation for studying these spectral properties comes from the theory of quantum chaos which deals with quantum systems exhibiting chaotic motion in the classical limit. One of the main observations of this field is that in the extreme case, when classical motion is strongly chaotic, and in the limit  $\hbar \rightarrow 0$ , the statistical properties of spectra are well described by random matrix theory (RMT). At the same time, the spectra of quantized integrable systems display Poissonian statistics. An important goal of quantum chaology is to develop a theory, which relates the quantum spectral statistics to the underlying features of classical dynamics. The main tool in this endeavour consists of trace formulae which provide an expression for the spectral density in terms of classical periodic manifolds—isolated orbits for chaotic systems and tori for integrable ones. In most cases, only the semiclassical approximations for the trace formulae are known [24] and their application is not only hampered by the intrinsic complexity of the set of periodic orbits, but also by the doubts about the ability of the semiclassical trace formulae to provide accurate enough basis for the further developments. This motivated the introduction and the study of particular “toy” systems where the required periodic-orbit data can be easily accumulated, while at the same time the trace formulae are exact rather than semiclassical [25]. Unfortunately, only very few models combine the desirable features of both behaving “typically” and being mathematically simple. It is the main purpose of this paper to propose quantum graphs as a very convenient and rich class of systems where the above mentioned requirements are met satisfactorily. We shall show that for quantum graphs, one can write an exact trace formula, which is based on “periodic orbits” in a way which is analogous to the known trace formulae for chaotic systems. Moreover, we shall define the corresponding underlying classical dynamics and write the relevant Frobenius Perron operator for the “phase space” evolution. This analogy will enable us to study further the connection between spectral fluctuations and the classical dynamics. Another clear advantage of quantum graphs is the relative ease by which a large number of spectral data can be computed. This enables rather accurate numerical studies of systems and problems for which analytical results are lacking or insufficient.

This paper extends our previous report [23] on the spectral properties of quantum graphs, both in detail and depth. In particular, we address issues which have to do with the transition which the spectral statistics undergo when the connectivity of the graph is altered. This problem is intimately connected with the semiclassical theory of Anderson localization. We also add another parameter to the model, which enables us to interpolate between Dirichlet and Neumann boundary conditions. We show that this induces a transition between integrable and chaotic dynamics, and we study its effect on the spectral statistics.

The paper is structured in the following way. In Section II, the mathematical model is introduced and the main definitions are given. In Section III we are describing three methods of quantizing graphs. The first method is rather standard (see, e.g., [16]) and it is the most convenient for numerical computations. The two other methods are related to the scattering approach to quantization [26]. One of them forms the basis for the development of the exact trace formula, and it singles out a unitary matrix of dimension  $2B \times 2B$  where  $B$  is the number of bonds on the graph. This matrix is the main building block of our theory, and we refer to it as the “bond scattering matrix”  $S_B$ . An alternative quantization condition is achieved in terms of the “vertex scattering matrix”  $S_V$ . It is of dimension  $V \times V$  where  $V$  is the number of vertices, and it describes the transport through a system in which each of the vertices is attached to a conducting wire. In Section IV we present the trace formula for the quantum graph and also express the spectral  $\zeta$  function as a sum over composite periodic orbits. Section IV terminates with the introduction and the discussion of the underlying classical system. In Section V, the statistical properties of the eigenphase spectrum of the bond scattering matrix  $S_B$  and of the energy (or wavenumber) spectrum are analyzed and compared with the predictions of RMT and of periodic orbits theory. In Section VI, we analyze two families of graphs which are not uniformly connected. The resulting spectral statistics deviate from the expectations of RMT, and we explain these deviations using periodic orbit theory. Within this study, we investigate also the localization/delocalization transition experienced by graphs as a function of the connectivity. Our conclusions are summarized in the last section (Section VII).

## II. QUANTUM GRAPHS: DEFINITIONS

In this section we shall present and discuss the Schrödinger operator for graphs. We start with a few definitions. Graphs consist of  $V$  vertices connected by  $B$  bonds (or edges). The valency  $v_i$  of a vertex  $i$  is the number of bonds meeting at that vertex. The graph is called  $v$ -regular if all the vertices have the same valency  $v$ . When the vertices  $i$  and  $j$  are connected, we denote the connecting bond by  $b = (i, j)$ . The same bond can also be referred to as  $\vec{b} \equiv (\text{Min}(i, j), \text{Max}(i, j))$  or  $\bar{b} \equiv (\text{Max}(i, j), \text{Min}(i, j))$  whenever we need to assign a direction to the bond. Several bonds connecting the same two vertices are called multiple bonds and the corresponding graph is called a multi-graph. Finally, a bond with coinciding endpoints is called a

*loop*. In what follows, unless explicitly specified, we shall consider graphs without multiple bonds or loops. Moreover, we shall treat only connected graphs.

Associated to every graph is its *connectivity (adjacency) matrix*  $C_{i,j}$ . It is a square matrix of size  $V$  whose matrix elements  $C_{i,j}$  are given in the following way

$$C_{i,j} = C_{j,i} = \begin{cases} 1 & \text{if } i, j \text{ are connected} \\ 0 & \text{otherwise} \end{cases}, \quad i, j = 1, \dots, V. \quad (1)$$

For loop-less graphs the diagonal elements of  $C$  are zero. The connectivity matrix of connected graphs cannot be written as a block diagonal matrix. The valency of a vertex is given in terms of the connectivity matrix by  $v_i = \sum_{j=1}^V C_{i,j}$  and the total number of bonds is  $B = \frac{1}{2} \sum_{i,j=1}^V C_{i,j}$ . As will be shown bellow (Subsection IV.C), the topological characterization of the graph which was given above is sufficient for the study of “classical dynamics” on graphs.

For the quantum description we assign to each bond  $b = (i, j)$  a coordinate  $x_{i,j}$  which indicates the position along the bond.  $x_{i,j}$  takes the value 0 at the vertex  $i$  and the value  $L_{i,j} \equiv L_{j,i}$  at the vertex  $j$  while  $x_{j,i}$  is zero at  $j$  and  $L_{i,j}$  at  $i$ . We have thus defined the *length matrix*  $L_{i,j}$  with matrix elements different from zero, whenever  $C_{i,j} \neq 0$  and  $L_{i,j} = L_{j,i}$  for  $b = 1, \dots, B$ . The derivations presented in the sequel are valid for any choice of the lengths  $L_{i,j}$ . However, in some applications we would avoid non-generic degeneracies by assuming that the  $L_{i,j}$  are *rationally independent*. The mean length is defined by  $\langle L \rangle \equiv (1/B) \sum_{b=1}^B L_b$ .

The wavefunction  $\Psi$  is a  $B$ -component vector and will be written as  $(\Psi_{b_1}(x_{b_1}), \Psi_{b_2}(x_{b_2}), \dots, \Psi_{b_B}(x_{b_B}))^T$  where the set  $\{b_i\}_{i=1}^B$  consists of  $B$  different bonds. We will call  $\Psi_b(x_b)$  the component of  $\Psi$  on the bond  $b$ . The bond coordinates  $x_b$  were defined above. When there is no danger of confusion, we shall use the shorthand notation  $\Psi_b(x)$  for  $\Psi_b(x_b)$  and it is understood that  $x$  is the coordinate on the bond  $b$  to which the component  $\Psi_b$  refers.

The Schrödinger operator (with  $\hbar = 2m = 1$ ) is defined on the graph in the following way [9, 16]: On each bond  $b$ , the component  $\Psi_b$  of the total wavefunction  $\Psi$  is a solution of the one-dimensional equation

$$\left(-i \frac{d}{dx} - A_b\right)^2 \Psi_b(x) = k^2 \Psi_b(x), \quad b = (i, j). \quad (2)$$

We included a “magnetic vector potential”  $A_b$  (with  $\Re e(A_b) \neq 0$  and  $A_{\bar{b}} = -A_b$ ) which breaks the time reversal symmetry. In most applications we shall assume that all the  $A_b$ ’s are equal and the bond index will be dropped.

The wavefunction must satisfy boundary conditions at the vertices, which ensure continuity (uniqueness) and current conservation. The imposition of these boundary conditions guarantees that the resulting Schrödinger operator is self-adjoint. The continuity condition requires that at each vertex  $i$ , the wavefunction assumes a value denoted by  $\varphi_i$  which is independent of the bond from where the vertex is approached. Current conservation imposes a condition on the derivatives of the

wavefunction at the vertices. By assuming that  $\{b_i\}_{i=1}^B = \{\vec{b}_i\}_{i=1}^B$  the conditions are explicitly specified in the following way. For every  $i = 1, \dots, V$ :

$$\left\{ \begin{array}{l} \bullet \text{ Continuity,} \\ \Psi_{i,j}(x)|_{x=0} = \varphi_i, \quad \Psi_{i,j}(x)|_{x=L_{i,j}} = \varphi_j \quad \text{for all } i < j \text{ and } C_{i,j} \neq 0 \\ \bullet \text{ Current conservation,} \\ \sum_{j < i} C_{i,j} \left( iA_{j,i} - \frac{d}{dx} \right) \Psi_{j,i}(x) \Big|_{x=L_{i,j}} \\ \quad + \sum_{j > i} C_{i,j} \left( -iA_{i,j} + \frac{d}{dx} \right) \Psi_{i,j}(x) \Big|_{x=0} = \lambda_i \varphi_i. \end{array} \right. \quad (3)$$

The parameters  $\lambda_i$  are free parameters which determine the boundary conditions. In many applications we shall assume that the  $\lambda_i$  are all equal, and in such cases the vertex index will be dropped. In the case when  $v_i = 2$ , the matching conditions can be represented by a  $\delta$ -function potential of strength  $\lambda_i$ . By analogy, we shall refer to the  $\lambda_i$  as the *vertex scattering potential*. In the sequel, we shall always assume that  $\lambda_i \geq 0$  and will consider the domain  $k^2 \geq 0$  (which excludes states bounded at a single vertex). The special case of zero  $\lambda_i$ 's corresponds to Neumann boundary conditions. Dirichlet boundary conditions are introduced when all the  $\lambda_i = \infty$ . This implies  $\varphi_i = 0$  for all  $i$ , thus turning the graph into a union of non interacting bonds. A finite value of  $\lambda_i$  introduces a new length scale. It is natural therefore to interpret it in physical terms as a representation of a local impurity or an external field [18, 19, 27]. We finally note that the above model can be considered as a generalization of the Kronig–Penney model to a multiply connected, yet one dimensional manifold.

### III. THE SPECTRUM OF QUANTUM GRAPHS

The set of boundary conditions (3), discussed in the previous section, ensures that the Schrödinger operator (2) is self-adjoint, and hence the existence of an unbounded, discrete spectrum  $\{k_n^2\}$ . In the following three subsections we shall introduce three different approaches which can be used for the calculation of the wavenumbers spectrum  $\{k_n\}$ . These approaches complement each other and enable us to address various aspects of the quantum graphs using different points of view.

#### A. The Vertex Secular Equation

The eigenfunctions of the graph are completely determined by their values at the vertices  $\{\varphi_i\}_{i=1}^V$ . The quantization condition which is to be derived here specifies the values of  $k$  for which a non trivial set of  $\{\varphi_i\}_{i=1}^V$ 's can be found [9, 16].

The wavefunction  $\Psi$  is constructed from  $B$  components which correspond to the various bonds. At any bond  $b = (i, j)$  the component  $\Psi_b$  can be written in terms of its values on the vertices  $i$  and  $j$  as

$$\Psi_{i,j} = \frac{e^{iA_{i,j}x}}{\sin kL_{i,j}} (\varphi_i \sin[k(L_{i,j} - x)] + \varphi_j e^{-iA_{i,j}L_{i,j}} \sin kx) C_{i,j}, \quad i < j. \quad (4)$$

$\Psi$  has, by construction, a unique value on the vertices and satisfies the Schrödinger Eq. (2). The current conservation condition (3) leads to

$$\begin{aligned} - \sum_{j < i} \frac{ke^{iA_{j,i}L_{i,j}} C_{i,j}}{\sin(kL_{i,j})} (-\varphi_j + \varphi_i e^{-iA_{j,i}L_{i,j}} \cos(kL_{i,j})) \\ + \sum_{j > i} \frac{kC_{i,j}}{\sin(kL_{i,j})} (-\varphi_i \cos(kL_{i,j}) + \varphi_j e^{-iA_{i,j}L_{i,j}}) = \lambda_i \varphi_i, \quad \forall i. \end{aligned} \quad (5)$$

This is a set of linear homogeneous equations for the  $\varphi$ 's which has a non-trivial solution when

$$\det(h_{i,j}(k, A)) = 0, \quad (6)$$

where

$$h_{i,j}(k, A) = \begin{cases} - \sum_{m \neq i} C_{i,m} \cot(kL_{i,m}) - \frac{\lambda_i}{k}, & i = j \\ C_{i,j} e^{-iA_{i,j}L_{i,j}} (\sin(kL_{i,j}))^{-1}, & i \neq j. \end{cases} \quad (7)$$

The terms  $h_{l,m} = h_{m,l}^*$ ,  $h_{l,l}$ , and  $h_{m,m}$  in (7) diverge when  $k$  is an integer multiple of  $\pi/L_{l,m}$ . This can be easily rectified by replacing the diverging terms by

$$\begin{aligned} h_{l,m}(k, A) &= h_{m,l}(k, A) = 0 \\ h_{l,l}(k, A) &= - \sum_{j' \neq m} C_{l,j'} \cot(kL_{l,j'}) - \frac{\lambda_l}{k}, \\ h_{m,m}(k, A) &= - \sum_{j' \neq l} C_{j',m} \cot(kL_{j',m}) - \frac{\lambda_m}{k}. \end{aligned} \quad (8)$$

The secular Eqs. (6)–(8) for the quantized graph can be solved numerically to provide an arbitrarily large sequence of eigenvalues  $\{k_n\}$ .

As we said previously, the effect of the Dirichlet boundary condition on all the vertices ( $\lambda_i = \infty$ ,  $\forall i$ ) is to disconnect the bonds. The eigenfunctions in this case have a simple structure: they vanish on all the bonds except on one of the bonds,  $b$ , where

$$\Psi_b = \frac{e^{iA_b x}}{\sqrt{L_b}} \sin\left(\frac{n_b \pi x}{L_b}\right), \quad k_n^{(b)} = \frac{n_b \pi}{L_b} \quad \text{for all } n_b > 0, \quad (9)$$

for all  $b$ . The spectrum is the union of the individual spectra, and when the lengths  $L_b$  are rationally independent, the resulting spectrum displays some Poissonian features. When the  $\lambda_i$  are large but finite there is always a small probability of “leaking” of the wavefunctions through the vertex scattering potential. As  $k$  increases, however, all intermediate boundary conditions converge to the Neumann limit.

### B. Scattering Approach—The Bonds $S_B$ Matrix

The quantization of graphs can be accomplished in a different way which although less efficient from the numerical point of view, provides us with a natural and convenient starting point for the construction of the trace formula. It is an example of the scattering approach to quantization [26]. Another variant of this method will be presented in the following subsection.

We first introduce the scattering matrix related to a single vertex. This is done by solving an auxiliary problem of a single vertex  $i$ , say, with  $v_i$  emanating bonds which extend to infinity. The wavefunction  $\Psi^{(i)}$  has components on all the bonds  $b_j \equiv (i, j)$ ,  $j = 1, \dots, v_i$ , which emerge from the  $i$  vertex (note that we enumerate and denote the bonds in the auxiliary problem by their analogues on the original graph).  $\Psi^{(i)}$  can be written as a linear combination of functions  $\Psi^{(i, j)}$  which are solutions for the case where there is an incoming wave entering  $i$  from  $b_j = (i, j)$  and outgoing waves from  $i$  to all bonds  $b_{j'}$  (including  $j = j'$  which correspond to the reflected part).  $\Psi^{(i, j)}$  is a  $v_i$ -dimensional vector with components  $\Psi_{j', j}^{(i, j)}(x_{j'})$  for all  $1 \leq j' \leq v_i$ ,

$$\Psi_{j'}^{(i, j)}(x_{j'}) = \delta_{j, j'} e^{-ikx_{j'} + iA_{i, j}x_{j'}} + \sigma_{j, j'}^{(i)} e^{ikx_{j'} + iA_{i, j'}x_{j'}}. \quad (10)$$

Here the  $x_{j'}$  are the distances from the vertex  $i$  along the bonds  $(i, j')$ , and  $\sigma_{j, j'}^{(i)}$  is the  $v_i \times v_i$  scattering matrix, which provides a transformation between the incoming and the outgoing waves at the vertex  $i$ . The matching conditions (3) at the vertex ( $x_j = 0$ ) together with (10), can be used to determine  $\sigma_{j, j'}^{(i)}$ :

$$\sigma_{j, j'}^{(i)} = \left( -\delta_{j, j'} + \frac{(1 + e^{-i\omega_i})}{v_i} \right) C_{i, j} C_{i, j'}, \quad \omega_i = 2 \arctan \frac{\lambda_i}{v_i k}. \quad (11)$$

For the Dirichlet boundary conditions we get  $\sigma_{j, j'}^{(i)} = -\delta_{j, j'}$  which indicates total reflection. For the Neumann boundary condition,  $\sigma_{j, j'}^{(i)} = -\delta_{j, j'} + (2/v_i)$  which is independent of  $k$ . For any intermediate boundary condition, the parameter that controls the scattering process is the  $k$  dependent parameter

$$A_i \equiv \frac{\lambda_i}{v_i k}. \quad (12)$$

The scattering matrix approaches the Neumann expression as  $k \rightarrow \infty$ . Note that in all the non trivial cases ( $v_i > 2$ ), back-scattering ( $j = j'$ ) is singled out both in sign

and in magnitude:  $\sigma_{j,j}^{(i)}$  has always a negative real part, and the reflection probability  $|\sigma_{j,j}^{(i)}|^2$  approaches 1 as the valency  $v_i$  increases. One can easily check that  $\sigma^{(i)}$  is a symmetric unitary matrix, ensuring flux conservation and time reversal symmetry at the vertex. For the Neumann boundary conditions  $\sigma^{(i)}$  is a real orthogonal matrix.

We now write the general expression for an eigenfunction of the quantum graph in terms of its components on the bonds  $b = (i, j)$ . We write the *same* bond wavefunction in two ways. First, we use the standard notation introduced before and call it  $\Psi_{i,j}(x_j)$  where  $x_j$  is the distance from  $i$ . The second representation employs the “time reversed” notation where the wavefunction is denoted by  $\Psi_{j,i}(x_i)$  and  $x_i$  is the distance from  $j$ . The general expressions for the wavefunction in the two representations read

$$\begin{aligned}\Psi_{i,j}(x_j) &= a_{i,j} e^{i(-k + A_{i,j})x_j} + b_{j,i} e^{i(k + A_{i,j})x_j} \\ \Psi_{j,i}(x_i) &= a_{j,i} e^{i(-k + A_{j,i})x_i} + b_{i,j} e^{i(k + A_{j,i})x_i} \\ &= a_{j,i} e^{i(k - A_{j,i})x_j} e^{i(-k + A_{j,i})L_{i,j}} + b_{i,j} e^{i(k + A_{j,i})L_{i,j}} e^{i(-k - A_{j,i})x_j}.\end{aligned}\quad (13)$$

The two representations describe the same function. This gives

$$b_{i,j} = a_{j,i} e^{-ikL_{i,j} - iA_{i,j}L_{i,j}}, \quad b_{j,i} = a_{i,j} e^{-ikL_{i,j} - iA_{j,i}L_{i,j}}. \quad (14)$$

In other words, but for a phase factor, the outgoing wave from the vertex  $i$  in the direction  $j$  is identical to the incoming wave at  $j$  coming from  $i$ . The incoming and outgoing components of the wavefunction impinging on the  $i$ th vertex satisfy

$$b_{i,j} = \sum_{j'} \sigma_{j,j'}^{(i)} a_{i,j'}. \quad (15)$$

Equations (14)–(15) can be combined to a set of  $2B$  homogeneous linear equations for the coefficients  $a_{i,j}$  which describe the wavefunction on each of the bonds.  $a_{i,j}$  is the amplitude for propagation from the  $i$  to  $j$  vertex along the bond  $b = (i, j)$ , while,  $a_{j,i}$  is the amplitude for the propagation in the “time reversed” direction (i.e., from  $j$  to  $i$ ) along the same bond. This distinction corresponds to assigning directions to the bonds, so that  $\vec{b}$  and  $\bar{b}$  are considered as different entities. We thus see that the present approach for quantizing the graph singles out the description in terms of *directed bonds* as the natural setup.

The condition for a non-trivial solution for the  $2B$  dimensional vector  $(a_{\vec{b}_1}, \dots, a_{\vec{b}_B}, a_{\bar{b}_1}, \dots, a_{\bar{b}_B})^T$  gives the secular equation for the total graph, of the form [21]

$$\zeta_B(k) = \det[I - S_B(k, A)] = 0. \quad (16)$$

Here, the “bond scattering matrix”  $S_B(k, A) = D(k, A) T$  is a unitary matrix in the  $2B$  dimensional space of directed bonds. It is a product of a diagonal unitary matrix  $D(k, A)$  which depends on the metric properties of the graph, and a unitary matrix  $T$  which depends on the connectivity and on the vertex scattering potentials.

$$D_{ij, i'j'}(k, A) = \delta_{i, i'} \delta_{j, j'} e^{ikL_{ij} + iA_{i,j}L_{ij}}; \quad \text{with } L_{ij} = L_{ji} \quad \text{and} \quad A_{ij} = -A_{ji} \quad (17)$$

$$T_{ji, nm} = \delta_{n, i} C_{j, i} C_{i, m} \sigma_{ji, im}^{(l)}.$$

The matrix elements of  $T$  assign an amplitude to a transition from one directed bond to another. Such a transition can occur only if the directed bonds are connected, that is, one is incoming and the other is outgoing from the same vertex. The phase and magnitude of the amplitude is given by the corresponding matrix element of the single vertex scattering matrix. From (16) it follows that  $k_n$  belongs to the wavenumber spectrum if and only if  $S_B(k_n, A)$  has an eigenvalue  $+1$ . As no approximations were made at any step of the derivation, this quantization condition is exact. Furthermore, this gives a constructive method to obtain not only the eigen-energies, but also the wavefunction, in terms of the eigenvector of  $S_B(k_n, A)$  with the eigenvalue  $+1$  [26].

The “bond scattering matrix”  $S_B$  cannot be associated with an actual scattering system in the usual sense of scattering theory. Nevertheless we shall keep referring to it as a scattering matrix, since it yields a quantization condition which is of the standard form in the scattering approach.

We finally comment that we use the letter  $\zeta_B$  to denote the secular function (16), because it can be cast in a form which is reminiscent of the Riemann–Siegel expression for the Riemann  $\zeta$  function on the critical line. This will be shown in Section IV.

### C. Scattering Approach—The Vertex $S_V$ Matrix

The vertex scattering matrix  $S_V$  is obtained by converting the graph of interest into a proper scattering system. This is done by attaching a lead which is extended to infinity at each of the graph vertices. A scattering solution with an incoming wave only in the lead  $l$  and outgoing waves on all the leads can be written in the following way. On the external leads,

$$\Psi_i^{(l)}(x) = \delta_{i, l} e^{-ikx} + (S_V)_{i, l} e^{ikx}. \quad (18)$$

On the  $B$  internal bonds,

$$\Psi_{i, j}^{(l)}(x) = \frac{C_{i, j} e^{iA_{i, j} x}}{\sin kL_{i, j}} (\varphi_i^{(l)} \sin[(L_{i, j} - x)k] + \varphi_j^{(l)} e^{-iA_{i, j} L_{i, j}} \sin kx), \quad i < j. \quad (19)$$

By applying the continuity and current conservation conditions (3) at all the vertices, we get

$$\varphi_i^{(l)} = \delta_{i, l} + (S_V)_{i, l}$$

$$(-\delta_{i, l} + (S_V)_{i, l}) i + \sum_{j=1}^V h_{i, j}(k) \varphi_j^{(l)} = 0, \quad (20)$$

where  $h(k)$  is the secular matrix defined in (7), (8). Combining the above two equations we finally get for  $S_V$

$$S_V = (iI + h(k))^{-1} (iI - h(k)), \quad (21)$$

where  $I$  is the  $V \times V$  unit matrix.

$S_V$  is unitary since  $h(k)$  is hermitian, which ensures current conservation. The graph spectrum can be identified as the set of wavenumbers for which  $S_V$  has 1 as an eigenvalue. This corresponds to a solution where no current flows in the leads so that the continuity equations are satisfied on the internal bonds (see [26]). Thus 1 is in the spectrum of  $S_V$  if

$$\zeta_V(k) \equiv \det[I - S_V] = 0 \leftrightarrow 2^V \det[iI + h(k)]^{-1} \det h(k) = 0 \quad (22)$$

which is satisfied once  $\det h(k) = 0$ . This is identical with the condition (6) which was derived in Subsection III.A.

Variations on the same theme can be obtained by considering graph scattering systems where leads are attached to an arbitrary set of  $L$  vertices  $\{i_l\}_{l=1}^L$ , with  $1 \leq L < V$ . The  $L \times L$  scattering matrix  $S_V$  has to be modified in the following way

$$S_V = 2iW(h(k) + iW^T W)^{-1} W^T - I, \quad (23)$$

where  $W_{i_l, j} = \delta_{i_l, j}$  is the  $L \times V$  leads - vertices coupling matrix. In the case that we examined previously with  $L = V$ ,  $W = I$ .

The matrices  $S_V$  will not be studied any further in this work, and the derivation above was given for the sake of completeness. The  $S_V$  scattering matrix corresponds to proper scattering problems and can be used to model experimental systems, such as, e.g., conductance of mesoscopic microdots. We shall study the statistics of conductance fluctuations, based on the vertex scattering matrices  $S_V$  in a separate publication [28].

#### IV. PERIODIC ORBITS, THE TRACE FORMULA, AND CLASSICAL DYNAMICS ON GRAPHS

In this section we derive an expression for the quantal density of states in terms of periodic orbits on the graph. A trace formula for the Laplacian on graphs was first presented by J.-P. Roth [17]. Our result (see also [23]) generalizes Roth's expression in several ways, and it is derived by means of a different approach. The key element in this theory is the concept of a periodic orbit on the graph, which we shall introduce at this point.

An *orbit* on the graph is an itinerary (finite or infinite) of successively connected *directed* bonds  $(i_1, i_2), (i_2, i_3), \dots$ . For graphs without loops or multiple bonds, this is uniquely defined by the sequence of vertices  $i_1, i_2, \dots$  with  $i_m \in [1, V]$  and

$C_{i_m, i_{m+1}} = 1$  for all  $m$ . An orbit is *periodic* with period  $n$  if for all  $k$ ,  $(i_{n+k}, i_{n+k+1}) = (i_k, i_{k+1})$ . The *code* of a periodic orbit of period  $n$  is the sequence of  $n$  vertices  $i_1, \dots, i_n$  and the orbit consists of the bonds  $(i_m, i_{m+1})$  (with the identification  $i_{m+n} \equiv i_m$ ). In this way, any cyclic permutation of the code defines the same periodic orbit.

The periodic orbits (PO) can be classified in the following way:

- *Irreducible periodic orbits*—POs which do not intersect themselves so that any vertex label in the code can appear at most once. Since the graphs are finite, the maximum period of irreducible POs is  $V$ . To each irreducible PO corresponds its time reversed partner whose code is read in the reverse order. The only code which is both irreducible and conjugate to itself under time reversal is the code corresponding to POs of period 2.

- *Reducible periodic orbits*—POs whose code is constructed by inserting the code of any number of irreducible POs at any position which is consistent with the connectivity matrix. All the POs of period  $n > V$  are reducible.

- *Primitive periodic orbits*—POs whose code cannot be written as a repetition of a shorter code.

After these preliminaries, we are set to derive the trace formula for the graphs. Once this is done, we shall show that one can define classical dynamics on the graph and that the periodic orbits on the graph are indeed the analogue of the periodic orbits of hyperbolic classical Hamiltonian systems.

### A. The Trace Formula

The starting point for the derivation is the secular equation (16). The function  $\zeta_B(k)$  is a complex valued function. It will be convenient to write it as a real amplitude times a phase factor. Denoting the eigenvalues of  $S_B(k, A)$  by  $e^{i\theta_l(k)}$  for  $l=1, \dots, 2B$  we get

$$\zeta_B(k) = \exp\left(\frac{i}{2}\Theta(k)\right) 2^{2B} \prod_{i=1}^{2B} \sin \frac{\theta_i(k)}{2}, \quad (24)$$

where  $\Theta(k)$  is

$$\begin{aligned} \Theta(k) &\equiv \frac{1}{i} \log(\det(-S(k, A))) = \sum_{i=1}^{2B} \theta_i(k, A) - 2B\pi \\ &= k\mathcal{L} + (B - V)\pi - 2 \sum_{i=1}^V \arctan(A_i). \end{aligned} \quad (25)$$

Here  $\mathcal{L} = 2 \sum_{b=1}^B L_b$  is twice the total length of the graph, and the  $A_i$  depend on the boundary conditions as defined in (12). Notice that the parameters  $A_b$  do not appear in the above expression. This is because the contributions of time reversed bonds are canceled pairwise.

The last product in (24) is real on the real  $k$  axis. Therefore, the imaginary part of its logarithmic derivative is a sum of delta distributions located where  $\zeta_B(k) = 0$ . Using the expansion

$$\log \det(I - S_B(k)) = - \sum_{n=1}^{\infty} \frac{1}{n} \operatorname{tr} S_B^n(k) \quad (26)$$

we obtain the following expression for the density of states

$$d(k) = \frac{1}{2\pi} \frac{d}{dk} \Theta(k) + \frac{1}{\pi} \lim_{\varepsilon \rightarrow 0} \Im m \frac{d}{dk} \sum_{n=1}^{\infty} \frac{1}{n} \operatorname{tr} S_B^n(k + i\varepsilon). \quad (27)$$

The first term on the right hand side of (27) corresponds to the smooth spectral density while the second one provides the fluctuating part.

The spectral counting function  $N(k)$  is given by

$$N(k) = \int_0^k d(k') dk'. \quad (28)$$

From (27) we have

$$N(k) = \bar{N}(k) + \frac{1}{\pi} \Im m \sum_{n=1}^{\infty} \frac{1}{n} \operatorname{tr}(S_B(k))^n, \quad (29)$$

where

$$\bar{N}(k) - \bar{N}(0) \equiv \frac{1}{2\pi} [\Theta(k) - \Theta(0)] = \frac{k\mathcal{L}}{2\pi} + \frac{V}{2} - \frac{1}{\pi} \sum_{i=1}^V \arctan(A_i). \quad (30)$$

This is the smooth part of the spectral counting function. The leading term involves the “volume”  $\mathcal{L}$  of our system, and it is independent on the boundary condition  $\lambda_i$ . The next two terms are due to the scattering potentials on the vertices. The contribution  $V/2$  is minus the value of the third term at  $k=0$ . For the Neumann boundary condition, the limit  $\lambda_i \rightarrow 0$  should be taken after the value  $k=0$  is substituted. For large  $k$  the last term is inversely proportional to  $k$  if  $\lambda_i \neq 0$ . Hence, the mean level density  $\bar{d} = \partial_k \bar{N}(k)$  is essentially constant, reflecting the fact that the graph is one dimensional. For the Neumann boundary conditions ( $\lambda_i = 0$ ),  $\bar{d}$  is independent of the wavenumber  $k$  and  $\bar{N}(0) = 1/2$  and

$$\bar{N}(k) = \frac{k\mathcal{L}}{2\pi} + \frac{1}{2}. \quad (31)$$

The oscillatory part of the counting function is expressed in terms of  $\text{tr}(S_B(k))^n$ . Using the definitions (17) and  $S=DT$  one can obtain the  $\text{tr}(S_B(k))^n$  directly as sums over  $n$ -periodic orbits on the graph

$$\text{tr}(S_B(k))^n = \sum_{p \in \mathcal{P}_n} n_p \mathcal{A}_p^r e^{i(kl_p + \Phi_p)r} e^{i(\mu_p \pi + \rho_p(k))r}, \quad (32)$$

where the sum is over the set  $\mathcal{P}_n$  of primitive POs whose period  $n_p$  is a divisor of  $n$ , with  $r = n/n_p$ .  $l_p = \sum_{b \in p} L_b$  is the length of the periodic orbit.  $\Phi_p = \sum_{b \in p} L_b A_b$  is the ‘‘magnetic flux’’ through the orbit. If all the parameters  $A_b$  have the same absolute size  $A$  we can write  $\Phi_p = Ab_p$ , where  $b_p$  is the directed length of the orbit.  $\mu_p$  is the number of vertices (with  $v_i \geq 2$ ) where back scattering occurs. At the other  $v_p$  vertices on the PO the scattering is not backwards. The number of back scatters from vertices with  $v_i = 1$  is  $n_p - (\mu_p + v_p) \geq 0$ . The amplitudes  $\mathcal{A}_p$  are given by

$$\mathcal{A}_p = \prod_{s=1}^{\mu_p} \left| \left( 1 - \frac{2}{v_s(1+iA_s)} \right) \right| \prod_{t=1}^{v_p} \left| \frac{2}{v_t(1+iA_t)} \right| \equiv e^{-(\gamma_p/2)n_p}, \quad (33)$$

where  $\gamma_p$  plays the role of the Lyapunov exponent. When  $\lambda_i \neq 0$ , the phase of each term is modified by adding

$$\rho_p(k) = \sum_{i=1}^{\mu_p} \arctan \left( \frac{2A_i}{v_i(1+A_i^2)} - 2 \right) - \sum_{i=1}^{v_p} \frac{\omega_i}{2} - \sum_{i=1}^{n_p - (\mu_p + v_p)} \omega_i. \quad (34)$$

Substituting (32) in (27) one gets an *exact* trace formula

$$d(k) = \frac{\mathcal{L}}{2\pi} + \frac{1}{\pi} \sum_{i=1}^V \frac{v_i \lambda_i}{(v_i k)^2 + \lambda_i^2} + \frac{1}{\pi} \sum_{p,r} \frac{l_p \cos(r(kl_p + \Phi_p + \mu_p \pi + \rho_p(k)))}{e^{(\gamma_p/2)n_p r}}. \quad (35)$$

The above formula bears a striking formal similarity to the well known exact Selberg trace formula [29] for modular domains on Riemann surfaces with constant negative curvature, to the Riemann Weyl relation for the Riemann zeros on the critical line and to the semi-classical Gutzwiller trace formula for chaotic Hamiltonian systems [24]. As we shall show in the sequel, the analogy between POs on the graph and periodic orbits in dynamical systems follows naturally from the classical dynamics which we associate with the graph. This analogy is strengthened by further evidence: The number of  $n$ -POs on the graph is  $1/n \text{tr } C^n$ , where  $C$  is the connectivity matrix. Since its largest eigenvalue  $\Gamma_c$  is bounded between the minimum and the maximum valency, i.e.,  $\min v_i \leq \Gamma_c \leq \max v_i$ , periodic orbits proliferate exponentially with topological entropy  $\approx \log \Gamma_c$ . The amplitudes  $\mathcal{A}_p$  which play the role of the stability amplitudes decrease exponentially with  $n$  but not enough to make the series for  $d(k)$  absolutely convergent (positive entropy barrier). Finally,  $\mu_p$  is the analogue of the Maslov index. Its origin is

topological, and it counts the number of non trivial back scatters along the PO. This can be expressed as the number of sequences of strings of the type  $\dots i_a, i_b, i_a \dots$  (with  $v_b > 2$ ) which appear in the code of the PO.

The distinguishing feature of the graph trace formula is the structure of the spectrum of lengths  $l_p$  of the periodic orbits which appear in (35). In contrast with the other systems mentioned above, the lengths are constructed as linear combinations (with integer coefficients) of the elementary bond lengths  $L_b$ . Hence, the lengths spectrum is characterized by a high degree of degeneracy. The degeneracy is not too important for POs of period  $n \leq V$ . As  $n$  increases, it becomes progressively dominant, and it is the main feature of the length spectrum for periodic orbits with  $n > 2B$ . The effects of this degeneracy are most apparent in the study of spectral statistics which will be discussed in the next section.

### B. Periodic Orbits Expression for the Spectral $\zeta$ Function

The spectral density (35) is not convenient to deal with, since it is not a proper function but, rather, a distribution. In this section we would like to cast the information which is stored in (35) in a different form and express it using periodic orbits.

The first method for achieving this goal is based on the identity (26), where the periodic orbit expression (32) for  $\text{tr } S_B^n$  is substituted, and the summation over the repetitions is carried out explicitly. One gets

$$\zeta_B(k) = \prod_p (1 - t_p); \quad t_p = e^{-(\gamma_p/2) n_p} e^{i(k l_p + A b_p)} e^{i(\mu_p \pi + \rho_p(k))}. \quad (36)$$

This expression as a product over primitive POs justifies the letter  $\zeta$  by which the secular function is denoted. This product does not converge on the real  $k$  axis because the number of primitive POs proliferates exponentially, with a topological entropy which approximately equals the mean Lyapunov exponent  $\gamma$ . Hence, the product (36) converges in the absolute sense only for  $\Im m k > \gamma/(2\langle L \rangle)$ . This is the “entropy barrier” for the  $\zeta_B$  function. As a matter of fact, the formal manipulations which were used to derive (36) are strictly justified beyond the entropy barrier.

A converging, well behaved expression for the  $\zeta_B$  function on the real  $k$  axis can be obtained, and it is the analogue of the Riemann Siegel expression for the Riemann  $\zeta$  on the critical line. To this end, we first note that the  $\zeta_B(k)$  function (16) is the characteristic polynomial of the matrix  $S_B(k)$

$$\zeta_B(z, k) = \det(zI - S_B(k)) = \sum_{l=0}^{2B} a_l(k) z^l \quad (37)$$

evaluated at  $z = 1$ . The coefficients  $a_n(k)$  satisfy an inversive symmetry relation which follows from the unitarity of the scattering matrix  $S_B(k)$

$$a_{2B-l}(k) = e^{i\Theta(k)} a_l^*(k). \quad (38)$$

Utilizing relation (38) one may rewrite (37) in a more convenient form

$$\zeta_B(z, k)|_{z=1} = 2e^{i(\Theta(k)/2)} \operatorname{Re} \left\{ e^{-i(\Theta(k)/2)} \left( \sum_{l=0}^{B-1} a_l + \frac{1}{2} a_B \right) \right\}. \quad (39)$$

We would like to emphasize that this form of the secular function  $\zeta_B(k)$  is due to the unitarity of  $S_B(k)$ . Thus, the removal of the contributions of terms with  $l > B$  in (39) is not only a practical saving of numerical effort, but also an expression of a basic property of the system.

Let us now consider the  $S_B(k)$  matrix at a given wavenumber  $k$ . Its spectrum is on the unit circle, i.e.,  $z = \exp(i\theta)$  and  $\zeta_B(e^{i\theta}, k)$  becomes a function of  $\theta$  which depends parametrically on  $k$ . Yet, the secular function (39) is not real for real  $\theta$ . It is useful to define another function which is real on the real  $\theta$  line and vanishes at  $\theta = \theta_l$ . Thus, we introduce the spectral determinant which is obtained from (37) by extracting a phase factor

$$\begin{aligned} Z(\theta, k) &= e^{-i((\Theta(k) + 2B\theta)/2)} \zeta_B(e^{i\theta}, k) = 2^{2B} \prod_{l=1}^{2B} \sin \left( \frac{(\theta_l(k) - \theta)}{2} \right) \\ &= 2 \operatorname{Re} \left\{ e^{-i((\Theta(k) + 2B\theta)/2)} \left( \sum_{l=0}^{B-1} a_l e^{il\theta} + \frac{1}{2} a_B e^{iB\theta} \right) \right\}. \end{aligned} \quad (40)$$

The function  $Z(\theta, k)$  serves a dual purpose. Setting  $\theta = 0$  it is a real secular equation for the graph. For a fixed value of  $k$  it is the secular function for the spectrum of  $S_B(k)$ .

To write  $Z(\theta, k)$  in terms of periodic orbits it is useful to recall Newton's identities [26]

$$a_l = -\frac{1}{l} \left( \operatorname{tr} S^l + \sum_{n=1}^{l-1} a_n \operatorname{tr} S^{l-n} \right), \quad l = 1, \dots, 2B. \quad (41)$$

The explicit dependence of the  $a_l$  on  $\operatorname{tr} S^n$  takes the form [26]

$$\begin{aligned} a_l &= -\frac{1}{l} \operatorname{tr} S_B^l \\ &= -\frac{1}{l} \sum_{\vec{l}} \frac{(-1)^n}{\prod_{i=1}^n l_i} \operatorname{tr} S_B^{l-l_1} \operatorname{tr} S_B^{l_1-l_2} \dots \operatorname{tr} S_B^{l_{n-1}-l_n} \operatorname{tr} S_B^{l_n}, \end{aligned} \quad (42)$$

where the summation is over all vectors  $\vec{l}$  with integer entries such that  $l > l_1 > l_2 > \dots > l_n \geq 1$ . By substituting further from (32) the  $\operatorname{tr} S_B^l$  we get an expression of the  $a_l$ , for  $l \leq B$  in terms of composite orbits [30, 31].

The form obtained above for the spectral  $\zeta$  function is reminiscent of the Riemann–Siegel approximation for the Riemann  $\zeta$  on the critical line. Here, however, it is an exact expression, and because of the fact that the density of states is constant, the number of terms appearing in the sum is independent of  $k$ .

### C. Classical Evolution

We introduced above the concept of orbits on the graph as strings of vertex labels whose ordering obeyed the required connectivity. This is a finite coding which is governed by a Markovian grammar provided by the connectivity matrix. In this sense, the symbolic dynamics on the graph is Bernoulli. So far, the orbits were used and discussed as formal symbols devoid of a *dynamical* origin. In the present section we shall introduce the classical dynamics which can be associated with a graph, and which complements the quantum dynamics on the graph. The classical dynamics makes use of the representation of the graph in terms of directed bonds. In the following sections we shall use the label  $b$  to refer to the *directed* bonds, so that  $b = 1, \dots, 2B$  and we shall denote the time reversed pairs by  $b = (i, j) ; \hat{b} = (j, i)$ .

We consider a classical particle which moves freely as long as it is on a bond. The vertices are singular points, and it is not possible to write down the analogue of the Newton equations at the vertices. Instead, one can employ a Liouvillian approach, based on the study of the evolution of phase-space densities. The phase space evolution operator assigns transition probabilities between phase space points, for which a quantum analogue can be found. The phase-space description will be constructed on a Poincaré section which is defined in the following way. Crossing of the section is registered as the particle encounters a vertex, thus the “coordinate” on the section is the vertex label. The corresponding “momentum” is the direction in which the particle moves when it emerges from the vertex. This is completely specified by the label of the next vertex to be encountered. In other words,

$$\left\{ \begin{array}{l} \text{position} \\ \text{momentum} \end{array} \right\} \Leftrightarrow \left\{ \begin{array}{l} \text{vertex index} \\ \text{next index} \end{array} \right\}.$$

The set of all possible vertices and directions is equivalent to the set of  $2B$  directed bonds. The evolution on this Poincaré section is well defined once we postulate the transition probabilities  $P_{ji \rightarrow ij'}^{(i)}$  between the directed bonds  $b = (j, i)$  and  $b' = (i, j')$ . To make the connection with the quantum description, we adopt the quantum transition probabilities, expressed as the absolute squares of the  $S_B$  matrix elements

$$P_{ji \rightarrow ij'}^{(i)} = |\sigma_{j,j'}^{(i)}(k, A)|^2 = \left| -\delta_{j,j'} + \frac{(1 + e^{-i\omega_i})}{v_i} \right|^2. \quad (43)$$

The phases  $\omega_i$  are given in (11). For the two extreme cases, corresponding to Neumann and Dirichlet boundary conditions, (43) results

$$\begin{aligned} P_{ji \rightarrow ij'}^{(i)} &= \left( -\delta_{j,j'} + \frac{2}{v_i} \right)^2, & \text{Neumann} \\ &= \delta_{j,j'}, & \text{Dirichlet.} \end{aligned} \quad (44)$$

The transition probability  $P_{j_i \rightarrow j'}^{(i)}$  for the Dirichlet case admits the following physical interpretation. The particle is confined to the bond where it started and thus the phase space is divided to non-overlapping ergodic components ( $\approx$  "tori"). For all other boundary conditions, the graph is dynamically connected.

The classical evolution (Frobenius Perron) operator  $U_{b, b'}$  between the bonds  $b, b'$  reads

$$U_{ij, nm} = \delta_{j, n} P_{ij \rightarrow jm}^{(j)}. \quad (45)$$

$U$  does not involve any metric information on the graph, and for Dirichlet or Neumann boundary conditions  $U$  is independent of  $k$ .

If  $\rho_b(t)$  denotes the probability to occupy the bond  $b$  at the (topological) time  $t$ , then we can write down a Markovian Master equation for the classical density:

$$\rho_b(t+1) = \sum_{b'} U_{b, b'} \rho_{b'}(t). \quad (46)$$

The unitarity of the graph scattering matrix  $S_B$  guarantees  $\sum_{b=1}^{2B} U_{b, b'} = 1$  and  $0 \leq U_{b, b'} \leq 1$ , so that the probability that the particle is on any bond is conserved during the evolution. The spectrum of  $U$  is restricted to the interior of the unit circle and  $v_1 = 1$  is always an eigenvalue with the corresponding eigenvector  $|1\rangle = (1/2B)(1, 1, \dots, 1)^T$ . In most cases, the eigenvalue 1 is the only eigenvalue on the unit circle. Then, the evolution is ergodic since any initial density will evolve to the eigenvector  $|1\rangle$  which corresponds to a uniform distribution (equilibrium). The rate at which equilibrium is approached is determined by the gap between the next largest eigenvalue and 1. However, there are some non generic cases, such as, e.g., bipartite graphs when  $-1$  belongs to the spectrum. In this case the asymptotic distribution is not stationary (see, for example, Section VII). If 1 is the only eigenvalue on the unit circle we have

$$\rho(t) \xrightarrow[t \rightarrow \infty]{} |1\rangle \quad (47)$$

with a mixing rate  $\ln |v_2|$  determined by  $v_2$ , the second largest eigenvalue of  $U$ . This is characteristic of a classically mixing system.

Of prime importance in the discussion of the relation between the classical and the quantum dynamics are the traces  $u_n = \text{tr}(U^n)$  which are interpreted as the mean classical probability to perform  $n$ -periodic motion. When only one eigenvalue  $v$  is on the unit circle, one has that  $u_n \xrightarrow[n \rightarrow \infty]{} 1$ . Then, we can obtain a classical sum-rule by substituting the periodic orbit expansion of  $u_n$ ,

$$u_n = \sum_{p \in P_n} n_p (|\mathcal{A}_p|^2)^r \xrightarrow[n \rightarrow \infty]{} 1. \quad (48)$$

Each periodic orbit is endowed with a weight  $|\mathcal{A}_p|^2$  defined in terms of the stability amplitudes (33). It is the probability to remain on the orbit. These weights are the counterparts of the stability weights  $|\det(I - M_p)|^{-1}$  for hyperbolic periodic orbits

in Hamiltonian systems, where  $M_p$  is the monodromy matrix. Graphs, however, are one dimensional and the motion on the bonds is simple and stable. Ergodic (mixing) dynamics is generated because at each vertex a (Markovian) choice of one out of  $v$  directions is made. Thus, *chaos on graphs originates from the multiple connectivity of the (otherwise linear) system.*

Using the expression (48) for  $u_n$  one can easily write down the complete thermodynamic formalism for the graph. Here, we shall only quote the periodic orbit expression for the Ruelle  $\zeta$  function

$$\begin{aligned} \zeta_R(z) &\equiv (\det(I - zU))^{-1} = \exp[-\text{tr}(\ln(I - zU))] \\ &= \exp\left[\sum_n \frac{z^n}{n} u_n\right] = \prod_p \frac{1}{(1 - z^{n_p} \exp(-n_p \gamma_p))}, \end{aligned} \quad (49)$$

where the product extends over all primitive periodic orbits and we have used the definitions of (33).

## V. SPECTRAL STATISTICS

So far we developed the spectral theory of graphs, pointing out the similarity between quantum graphs and more complex quantum systems which display chaotic dynamics in the classical limit. In the present section we shall report about analytical and numerical results which show that the spectral statistics of these simple systems also follow the pattern of more general Hamiltonian systems. Namely, when the classical graph dynamics is mixing, and in the limit when the (topological) time needed to reach equilibrium is much shorter than the number of directed bonds, the spectral statistics for quantum graphs are very well reproduced by the predictions of Random Matrix Theory. In the integrable limit (Dirichlet boundary conditions) the graph spectral statistics is Poisson as is the case in generic integrable Hamiltonian systems. The investigation of the universality of spectral fluctuations and deviations thereof is especially convenient for graphs because of the transparent and simple spectral theory in terms of POs and because of the relative numerical ease by which large spectral data bases can be constructed. The parameters which appear in the theory can be used to study various characteristic spectral transitions: Changing the vertex potential parameters  $\lambda_i$  (which, for simplicity, we will choose to be the same for all the vertices i.e.,  $\lambda = \lambda_i$ ) induces the transition between classical integrability to chaos. This is accompanied by a spectral transition from Poisson to RMT like statistics. The parameter  $A_b$  (again for the sake of clarity we will choose  $|A_b| = A$  for all the bonds) allows us to break time reversal symmetry, and the mean valency can be used to study the dependence of spectral statistics on connectivity. All these questions will be dealt with in the present section.

The spectral theory presented above relied heavily on the bond scattering matrix  $S_B$  which provided the foundation for the periodic orbits theory and the connection

to the classical evolution. The spectral statistics of the eigenphases of the  $S_B$  matrix are also intimately connected with the spectral statistics of the graph wavenumber spectrum. Therefore, we will start our presentation by discussing the  $S_B$  matrix spectral statistics.

### A. The Spectral Statistics of the $S_B$ Matrix

We consider the  $S_B(k, A)$  matrices defined in (16), (17). Their spectra consist of  $2B$  points confined to the unit circle (eigenphases). Unitary matrices of the type considered here are commonly studied since they are the quantum analogues of classical, area preserving maps. Their spectral fluctuations depend on the nature of the underlying classical dynamics [32]. The quantum analogue of classically integrable maps display Poissonian statistics while in the opposite case of classically chaotic maps, the eigenphases statistics conform quite accurately with the results of RMT for Dyson's *circular ensembles*. The ensemble of unitary matrices which will be used for the statistical study will be the set of matrices  $S_B(k, A)$  with  $k$  in the range  $|k - k_0| \leq \Delta_k/2$ , where the mid-point  $k_0$  and the interval size  $\Delta_k$  are to be determined. Since the dimension of the  $S_B$  matrices is independent of  $k$ , the mean value  $k_0$  is important only when the boundary conditions are neither Neumann nor Dirichlet. For the intermediate boundary conditions,  $k_0$  sets the mean value of the parameter  $A$  (12), and  $\Delta_k$  must be chosen such that  $A$  does not change appreciably in the interval. However,  $\Delta_k$  must be much larger than the correlation length between the matrices  $S_B(k, A)$ . One can estimate the correlation length by studying the auto-correlation function

$$C(\chi) \equiv \frac{1}{\Delta_k} \int_{k_0 - \Delta_k/2}^{k_0 + \Delta_k/2} \frac{1}{2B} \text{tr} \left( S_B^\dagger \left( k' + \frac{\chi}{2} \right) S_B \left( k' - \frac{\chi}{2} \right) \right) dk'. \quad (50)$$

For the two extreme cases of Neumann and Dirichlet boundary conditions the auto-correlation function (50) can be calculated exactly. By writing the scattering matrix as  $S_B(k) = \exp(ikL) S_B(0)$  and substituting in (50) we find

$$C(\chi) = \frac{1}{B} \sum_{i=1}^B e^{iL_b \chi} = \int e^{iL \chi} P(L) dL \equiv \hat{P}(\chi), \quad (51)$$

where  $\hat{P}(\chi)$  is the Fourier transform of the probability distribution  $P(L)$  of the lengths of the bonds. Thus, the correlation is inversely proportional to the variance of the distribution of the lengths  $L_b$ . From now on, we shall assume  $\Delta_k \gg \text{var}(L_B)$ , which justifies the  $k$  averaging procedure. The ensemble average will be denoted by

$$\langle \cdot \rangle_k \equiv \frac{1}{\Delta_k} \int_{k_0 - \Delta_k/2}^{k_0 + \Delta_k/2} \cdot dk. \quad (52)$$

Another way to generate an ensemble of graphs is by randomizing the length matrix  $L$  which contains the lengths of the bonds while the connectivity (topology

of the graph) is kept constant. This is the disorder approach, which will also be applied when called for.

In the following Subsections VI.A.1–2, we investigate some statistical measures of the eigenphases  $\{\theta_l(k)\}$  of the scattering matrix  $S_B$  [33, 34] and compare them with the predictions of RMT and with the results of the periodic orbits theory of spectral fluctuations which was originally developed for quantized maps. The two statistics which we shall investigate are the spectral form factor and the autocorrelation of the spectral  $\zeta$  function. Explicit expressions for these quantities are given by Random Matrix Theory [35] and a semiclassical theory is also available [36–38].

### 1. The Form Factor

The  $S_B$  matrix for a fixed eigenvalue  $k$  is a unitary matrix with eigenvalues  $e^{i\theta_l(k)}$ . The spectral density of the eigenphases then reads

$$d(\theta; k) \equiv \sum_{l=1}^{2B} \delta(\theta - \theta_l(k)) = \frac{2B}{2\pi} + \frac{1}{2\pi} \sum_{n=1}^{\infty} e^{-i\theta n} \text{tr} S_B(k)^n + \text{c.c.}, \quad (53)$$

where the first term on the r.h.s is the smooth density  $\bar{d} = 2B/2\pi$ , while the others describe the fluctuating part.

The two-point correlations are expressed in terms of the excess probability density  $R_2(r)$  of finding two phases at a distance  $r$ , where  $r$  is measured in units of the mean spacing  $2\pi/2B$

$$R_2(r; k_0) = \frac{2}{2\pi} \sum_{n=1}^{\infty} \cos\left(\frac{2\pi r n}{2B}\right) \frac{1}{2B} \langle |\text{tr} S_B^n|^2 \rangle_k. \quad (54)$$

The form factor  $K(n, 2B) = (1/2B) \langle |\text{tr} S_B^n|^2 \rangle_k$  is the Fourier transform of  $R_2(r, k_0)$ . For a Poisson spectrum,  $K(n, 2B) = 1$  for all  $n$ . RMT predicts that  $K(n, 2B)$ , depends on the scaled time  $n/2B$  only [32], and explicit expressions for the orthogonal and the unitary circular ensembles are known [35].

We computed  $(1/2B) \langle |\text{tr} S_B^n|^2 \rangle_k$  for well connected graphs, with various vertex potential parameters. In Fig. 1 we show typical examples, calculated for a fully connected pentagon. The results for Neumann boundary conditions show quite a good agreement with the predictions of RMT for the circular ensembles. We shall discuss and explain these results in the following paragraphs.

To begin, consider the data for Neumann boundary conditions and  $A=0$  or  $A \neq 0$  (see Fig. 1). The predictions of RMT are also shown, and they reproduce quite well the smooth trend of the data in the two cases. The deviations from the smooth curves are not statistical and cannot be ironed out by further averaging. Rather, they are due to the fact that the graph is a dynamical system which cannot be described by RMT in all detail. To study this point in depth we shall express the form factor in terms of the PO expression (32). Assuming Neumann boundary conditions for the time being,

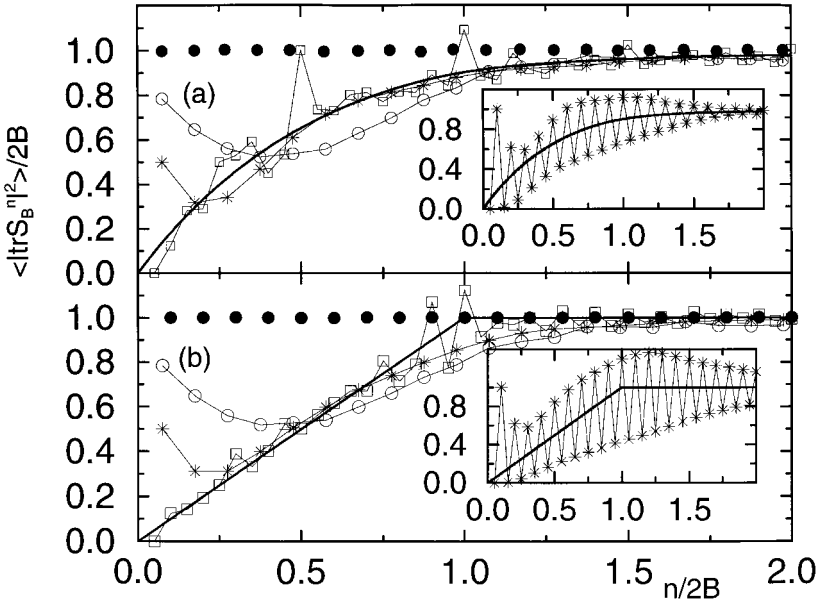


FIG. 1. The form factor for the eigenphase spectrum of  $S_B$  for a pentagon graph. Bold solid lines are the expectations for the COE and CUE expressions. The data are averaged over odd-even powers of the form factor as explained in the text. In the insets we present the form factor for the case  $A = 0.833$  ( $\circ$ ) without averaging. (a)  $A = 0$ ,  $A = 0$  ( $\square$ );  $A = 1.25$  ( $*$ );  $A = 2.5$  ( $\circ$ ); and  $A = 3500$  ( $\bullet$ ). (b)  $A \neq 0$  with the same boundary conditions as in (a).

$$\begin{aligned}
 \frac{1}{2B} \langle |\text{tr} S_B^n(k)|^2 \rangle_k &= \frac{1}{2B} \left\langle \left| \sum_{p \in \mathcal{P}_n} n_p \mathcal{A}_p^r e^{i(kl_p + Ab_p + \pi\mu_p)r} \right|^2 \right\rangle_k \\
 &= \frac{1}{2B} \sum_{p, p' \in \mathcal{P}_n} n_p n_{p'} \mathcal{A}_p^r \mathcal{A}_{p'}^{r'} \\
 &\quad \times \exp\{iA(rb_p - r'b_{p'}) + i\pi(r\mu_p - r'\mu_{p'})\} \Big|_{r'l_p = r'l_{p'}}. \quad (55)
 \end{aligned}$$

The  $k$  averaging is carried out on such a large interval that the double sum above is restricted to pairs of periodic orbits which have exactly the same length. The fact that we chose the lengths of the bonds to be rationally independent will enter the considerations which follow in a crucial way. Consider first the domain  $1 < n \ll 2B$ . The POs are mostly of the irreducible type, and the length restriction limits the sum to pairs of orbits which are conjugated under time reversal. Neglecting the contributions from repetitions and from self tracing orbits we get

$$\frac{1}{2B} \langle |\text{tr} S_B^n(k)|^2 \rangle_k \approx \frac{1}{2B} \sum_{p \in \mathcal{P}_n} n^2 \mathcal{A}_p^2 4 \cos^2 Ab_p = \frac{2n}{2B} u_n \langle \cos^2 Ab_p \rangle_n. \quad (56)$$

The classical return probability  $u_n$  approaches 1 as  $n$  increases (see (48)). However, deviations from unity reflect the fact that the classical dynamics reaches the ergodic state only after some time. The deviation which is simplest to understand occurs at  $n = 1$ . Since there are no classical fixed points (no self connected vertices) on the graph,  $u_1 = 0$ . However, in the limit  $B \rightarrow \infty$ , the short time deviations converge to the origin when the scaled form factor is studied. Neglecting the short time deviations, we can replace  $u_n$  by 1, and we see that the remaining expression to be evaluated is the classical expectation of  $\cos^2 Ab_p$  over POs of length  $n$ . For  $A = 0$  this factor is identically 1 and one obtains the leading term of the COE expression for  $n \ll 2B$ . If  $A$  is sufficiently large  $\langle \cos^2 Ab_p \rangle_n \approx 1/2$ , and one obtains the short time limit of the CUE expression. The transition between the two extreme situations is well described by

$$\langle \cos^2 Ab_p \rangle_n \approx \frac{1}{2}(e^{-A^2 \langle L_b^2 \rangle n/2} + 1). \tag{57}$$

This formula is derived by assuming that the total directed length  $b_p$  of a periodic orbit is a sum of elementary lengths with random signs.

One cannot use the arguments presented above for the range  $n \geq B$ . As  $n$  approaches  $B$  the degeneracy of the length spectrum prevails and for  $n > 2B$  all the orbits are degenerate. In other words, the restriction  $r l_p = r' l_{p'}$  in (55) does not pick up a unique orbit and its time reversed partner, but rather, a group of isometric but distinct orbits. Therefore, the interferences of the contributions from the group of all the orbits must be calculated. The relative sign of the terms is determined by the ‘‘Maslov’’ index. This can be seen better, once rewriting (55) in the form (we assume for simplicity  $A = 0$ )

$$\frac{1}{2B} \langle |\text{tr } S_B^n(k)|^2 \rangle_k = \frac{1}{2B} \sum_{\{q\}} \left| \sum_{p \in \mathcal{P}_q} n_p \mathcal{A}_p^r e^{i\pi \mu_p r} \right|^2, \tag{58}$$

where the second sum is over the set  $\mathcal{P}_q$  of PO of the type  $l_p = \sum q_b L_b$  with  $\sum q_b = n_p$ . It is clear that the indices of different orbits in a family of isometric POs are *correlated*. Otherwise, if the Maslov indices are random, one would regain the diagonal approximation (56) for arbitrarily long times. The correlations between the Maslov indices within the family of isometric POs are the analogue of action correlations in the semiclassical theory of spectral statistics [39]. The dynamical origin of these correlations is not known also for graphs, and it is one of the important open problems that should be addressed.

Graphs with Dirichlet boundary conditions are integrable in the sense explained above. One expects therefore that the spectral statistics in this case is Poissonian, which implies

$$\frac{1}{2B} \langle |\text{tr } S_B^n(k)|^2 \rangle_k = 1 \quad \text{for all } n > 1. \tag{59}$$

In the Dirichlet case, the  $S_B$  matrix reduces to a block diagonal form where each bond and its time reversed partner are coupled by a  $2 \times 2$  matrix of the form

$$S^{(b)}(k, A) = \begin{pmatrix} 0 & e^{i(k+A)L_b} \\ e^{i(k-A)L_b} & 0 \end{pmatrix}. \quad (60)$$

The spectrum of each block is the pair  $\pm e^{ikL_b}$ , with the corresponding symmetric and antisymmetric eigenvectors  $(1/\sqrt{2})(1, \pm 1)$ . As a result, we get

$$\frac{1}{2B} \langle |\text{tr } S_B^n(k)|^2 \rangle_k = 1 + (-1)^n \quad \text{for all } n \geq 1. \quad (61)$$

This deviation from the expected Poissonian result is due to the fact that the extra symmetry reduces the  $S_B$  matrix further into the symmetric and antisymmetric subspaces. The spectrum in each is Poissonian, but when combined together, the fact that the eigenvalues in the two spectra differ only by a sign is the reason for the anomaly (61). In the sequel we shall remove this feature by considering the smooth form factor obtained by taking the mean of successive  $n$  values.

The transition between the two extreme boundary conditions can be affected by using the interpolating boundary conditions where  $\lambda \neq \{0, \infty\}$ . The relevant parameters are the  $A$  defined in (12), and it is expected that the spectral statistics make the transition from RMT like to Poisson as these parameters span their range of values. The exact symmetry which prevails in the Dirichlet case is broken for intermediate values of  $A$ . However, the tendency towards trapping in a single bond is a dynamical feature, which persists for finite  $A$  values, and therefore the even-odd staggering of the form factor can be observed also for the intermediate range of  $A$  values (see inset in Fig. 1). Since the dynamical reason for this effect is clearly understood, we show in Fig. 1 the pairwise averaged form factor, which displays clearly the transition from the Poissonian to the RMT (COE and CUE) limit.

As was mentioned above, the short times deviations of the data from the RMT expectations (see Fig. 1) are real and are due to the deterministic nature of the dynamics induced by the  $S_B$  matrices. It is easy to show this explicitly for  $\langle |\text{tr } S^2|^2 \rangle$ , since here all the contributions are due to period-2 POs which are self tracing, and each has its distinct length. Using (32) we get

$$\frac{1}{2B} \langle |\text{tr } S_B^2(k)|^2 \rangle_k = 2 \left( \frac{(1 - (2/v))^2 + A^2}{1 + A^2} \right)^2, \quad (62)$$

independently of the value of  $A$ . This is different from the value  $1/B$  expected for the CUE and  $\approx 2/B$  expected for the COE.

## 2. Spectral $Z$ Function Correlations

We conclude this section with an analysis of the spectral  $Z$  function given by (40). The statistical properties of this function can be expressed in terms of the statistics of either the eigenphases  $\theta_l$  or the coefficients  $a_l$  (see (40)). Since the two

sets of variables are functionally related, they are statistically equivalent. In practice, however, one cannot check the full spectral distribution, and therefore it is advantageous to study statistical measures which are based on other accessible quantities. The measure which was proposed in [37, 40] was the autocorrelation function

$$\begin{aligned}
 C_Z(\eta) &\equiv \int_0^{2\pi} \left\langle Z\left(\theta + \frac{\eta}{2}; k\right) Z^* \left(\theta - \frac{\eta}{2}; k\right) \right\rangle_k \frac{d\theta}{2\pi} \\
 &= \sum_{l=0}^{2B} \langle |a_l|^2 \rangle_k e^{i\eta(l-B)}.
 \end{aligned}
 \tag{63}$$

This statistical measure depends on higher order correlations of the eigenphases. Hence,  $C_Z(\eta)$  tests aspects of the eigenvalues distribution which are not accessible by the study of the two-point form factor discussed previously.

The ensemble averages  $\langle |a_l|^2 \rangle$  for Circular Random Matrices were calculated in [35]. We shall quote here the results for the COE and CUE ensembles:

$$\begin{aligned}
 \langle |a_l|^2 \rangle_\beta &= 1 + \frac{l(2B-l)}{2B+1}, & \beta = 1 \\
 &= 1, & \beta = 2.
 \end{aligned}
 \tag{64}$$

An approximate expression for the  $\langle |a_l|^2 \rangle$  was obtained by assuming that the  $\text{tr } S^n$  are independent random Gaussian variables for  $n < B$  [37]. This approximation is an extension of the diagonal approximation mentioned above, and it leads to the following recursion relation

$$\langle |a_l|^2 \rangle = \frac{1}{l} \sum_{n=1}^l \langle |a_{l-n}|^2 \rangle \frac{\langle |\text{tr } S_B^n|^2 \rangle}{n}.
 \tag{65}$$

For the calculation of the autocorrelation function (63), it is sufficient to obtain the  $\langle |a_l|^2 \rangle$  for  $l \leq B$ . The rest are provided by the inverse symmetry (38) which moreover implies that the Fourier components of  $C_Z(\eta)$  are symmetric about  $B$  and thus the autocorrelation function is real.

Using the approximate result (56) for the form factor  $\langle |\text{tr } S_B^n|^2 \rangle \simeq gnu_n$  we have [40]

$$\langle |a_l|^2 \rangle = \frac{g}{l} \sum_{k=1}^l \langle |a_{l-k}|^2 \rangle u_k,
 \tag{66}$$

which should be solved with the initial condition  $\langle |a_0|^2 \rangle = 1$ . In (66),  $g = 2(1)$  for systems with (without) time reversal symmetry, and  $u_k = \text{tr } U^k$  is the classical return probability. For systems which display strong mixing,  $u_n = 1$ , and the approximate recursion relations reproduce the RMT result for systems which violate time reversal symmetry ( $\beta = 2$ ). For systems which are invariant under time reversal, one reproduces only the leading term in  $n/2B$  of the RMT result ( $\beta = 1$ ).

We computed numerically the  $\langle |a_l|^2 \rangle_k$  for the completely connected pentagon, subject to Neumann boundary conditions, where time reversal symmetry was either respected ( $A=0$ ) (Fig. 2a), or violated ( $A \neq 0$ ) (Fig. 2b). The results are displayed in Fig. 2, and they deviate substantially from the RMT predictions (64). Note that the values of  $\langle |\text{tr } S_B^n|^2 \rangle_k$  for the same system showed a rather good agreement with RMT (see Fig. 1). The reason for the large deviation is clear. No physical system can reproduce the strong mixing condition  $u_n = 1$  for all  $n$ . Indeed, this is the reason why  $\langle |\text{tr } S_B^n|^2 \rangle_k$  deviate from the RMT results for short times. Because of the iterative procedure (66), the short time non-generic effects reveal themselves in the higher order coefficients  $a_l$ , and this is why this statistical measure is much more sensitive to the non-universal features of the classical dynamics. The approximate theory presented above includes the correct short time behavior of the system, and therefore it reproduces the main features of the numerical data much better than RMT. A quantitative measure for the expected deviation from the RMT prediction can be given by the magnitude of the next to the leading eigenvalue of the classical evolution operator  $U$ . For the system we studied, it is  $-0.25$ , which is still far from the value 0 expected in the strong mixing limit.

Let us finally comment on the transition from Poisson to RMT due to variation of the parameters  $A_i$ . As it was mentioned already in the Introduction, for integrable systems, we expect that the spectrum is uncorrelated and described by the Poisson ensemble which gives for the  $\langle |a_l|^2 \rangle$  the expression

$$\langle |a_l|^2 \rangle = \binom{2B}{l}. \quad (67)$$

On the other hand, the diagonal approximation predicts that  $\langle |\text{tr } S^n|^2 \rangle \simeq 2B$  (see the previous section) and thus it provides us with the following recursion relation for the coefficients  $\langle |a_l|^2 \rangle$

$$\langle |a_l|^2 \rangle = \frac{2B}{l} \sum_{n=1}^l \frac{\langle |a_{l-n}|^2 \rangle}{n}. \quad (68)$$

In Figs. 2a, 2b, we present our numerical results for a fully connected pentagon and for various values of the parameter  $A$ . Again, we see that our system undergoes a transition from COE/CUE to Poisson statistics when  $A$  increases.

### B. Level Statistics

The statistical properties of the energy levels (or the wavenumbers) spectrum can be derived from the statistics of the eigenphases of  $S_B$  because of the following reasoning. The wavenumber spectral density can be written as

$$d(k) = \sum_{n=1}^{\infty} \delta(k - k_n) = \sum_{l=1}^{2B} \delta_{2\pi}(\theta_l(k)) \left| \frac{d\theta_l(k)}{dk} \right|. \quad (69)$$

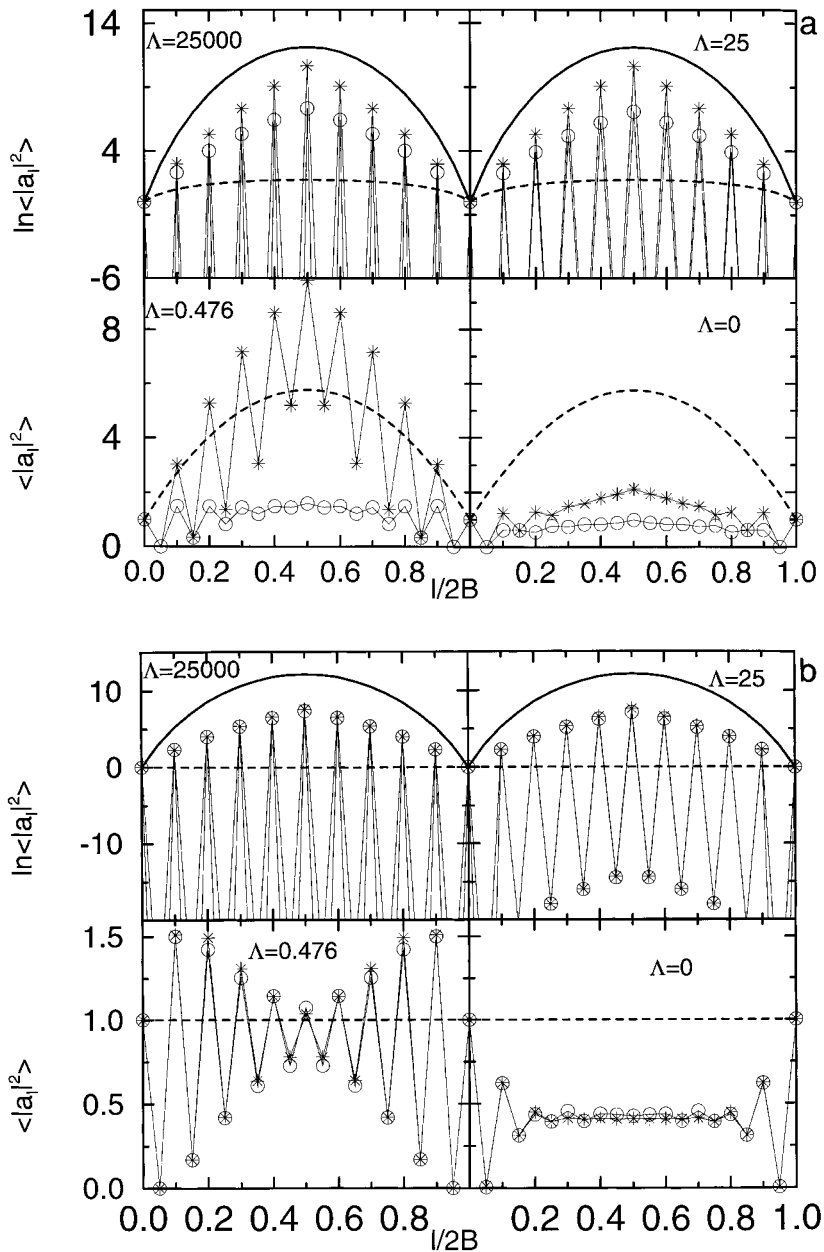


FIG. 2. The Fourier components  $\langle |a_l|^2 \rangle$  of  $C_Z$  for a pentagon graph. (\*) corresponds to semi-classical calculations while ( $\circ$ ) to the exact quantum mechanical calculations. (a)  $A=0$ ,  $A=25000$ ,  $A=25$ ,  $A=0.476$ , and  $A=0$ ; (b)  $A \neq 0$ , with the same boundary conditions. In both figures the bold solid line corresponds to Poisson while the bold dashed line is the expectation of the corresponding RMT.

One can easily show that

$$L_{min} \leq \frac{d\theta_l(k)}{dk} \leq L_{max}, \quad (70)$$

where  $L_{min, max}$  denote the minimal or the maximal bond length of the graph. Consider an interval  $\delta k$  about  $k_0$  so that  $\langle d\theta_l(k)/dk \rangle_l \delta k = \langle L \rangle \delta k < 2\pi$ . Since the mean wavenumber spectral density is  $\langle L \rangle B/\pi$  the interval  $\delta k$  can accommodate a large number of levels when  $B$  is large. The wavenumber density in the  $\delta k$  vicinity of  $k_0$  is

$$\begin{aligned} d(k; k_0) &= \sum_{l=1}^{2B} \delta_{2\pi} \left( \theta_l(k_0) + (k - k_0) \frac{d\theta_l(k)}{dk} \right) \frac{d\theta_l(k)}{dk} \\ &\approx \langle L \rangle \sum_{l=1}^{2B} \delta_{2\pi}(\theta_l(k_0) + (k - k_0)\langle L \rangle). \end{aligned} \quad (71)$$

For a given  $k$  value, the expression on the r.h.s. is the eigenphase density of the unitary matrix  $S_B(k_0)$  (the  $l$  independent shift of the phases does not change the distribution of intervals on the circle). Hence, one can read the short range statistical properties of the  $k$  spectrum, from the results on the statistics of the eigenphases which were discussed in the previous section. In the sequel we shall supply numerical data and additional arguments to show that this is indeed the case. We shall also compute various statistical measures which are commonly used in the statistical analysis of spectral fluctuations of quantum systems whose classical analogue is chaotic. We shall show that the spectrum of the quantized graph behaves as a typical member of this set of “quantum-chaotic” systems.

For the numerical calculation of the spectrum we had used the method described in Subsection III.A. That is, we identified the spectrum as the zeros of  $\det h(k, A)$ . The completeness of the spectrum was checked by comparing the counting function  $N(k)$  with Weyl’s law (30). An efficient detector of missing or spurious levels is provided by the function  $\delta_n$

$$\delta_n = N(k) - \bar{N}(k). \quad (72)$$

This quantity is expected to fluctuate around zero and a redundant or a missing eigenvalue is accompanied by an offset by  $\pm 1$ . Figure 3 shows a typical plot of  $\delta_n$  as a function of  $n$  for a graph containing 5 vertices (see inset in Fig. 3) and Neumann boundary conditions.  $\delta_n$  fluctuates about 0 as expected, with  $|\delta_n| < 2$  which is a quantitative indication of the rigidity of the spectrum. This is the behavior expected for a quantum chaotic system.

The spectral fluctuations are best studied in terms of the unfolded spectrum  $\{x_n\}$

$$x_n = \bar{N}(k_n) \quad (73)$$

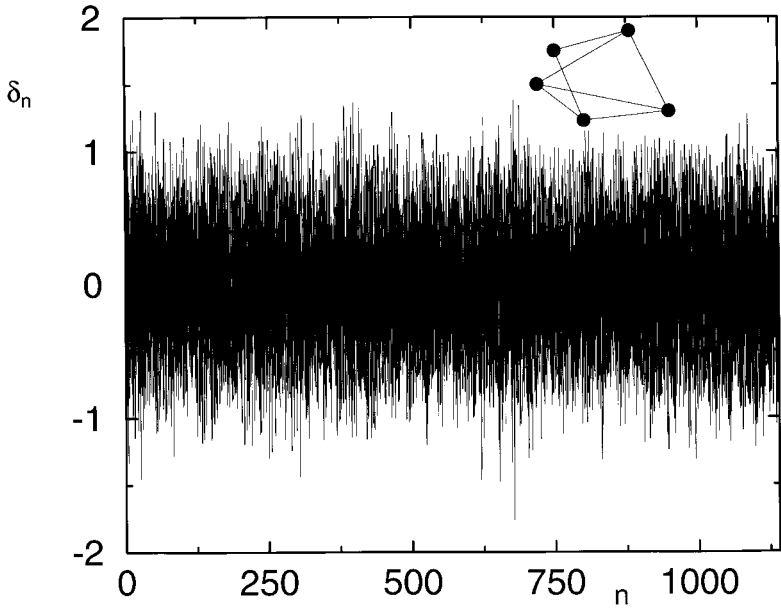


FIG. 3.  $\delta_n = N(k) - \bar{N}(k)$  vs the wavenumber label  $n$  for the graph shown in the inset.

whose mean level spacing is unity. Since (30) provides an exact expression for  $\bar{N}(k)$  the unfolding procedure is straightforward.

### 1. Level Spacing Distribution

The distribution  $P(s)$  of the spacings  $s_n = x_{n+1} - x_n$  of adjacent quantal levels (or its integrated form  $I(s) = \int_0^s P(r) dr$ ) is the most convenient and commonly used statistics. The expressions for  $P(s)$  for the Poisson, GOE, and GUE ensembles are well known and have been compared with the distributions derived from the graph spectra. The numerical results for many systems show that the graphs follow the general trend observed for realistic systems. As a typical example, the results for the fully connected quadrangle with Neumann boundary conditions ( $\lambda_i = 0$ ) and with  $A = 0$  and  $A \neq 0$  are shown in Fig. 4. They are based on the leading 80,000 eigenvalues for each case. We would like to emphasize that the spectra were calculated for a fixed set of bond lengths, in other words, no disorder averaging was employed. The agreement with the exact (not the Wigner surmise) RMT curves is very good [41], although systematic deviations at the level of 1% or less can be discerned (see inset of Fig. 4). These differences exceed the statistical error margin, and we believe that they originate from the fact that the short time dynamics on the graph does not follow the universal pattern, as was explained in the previous section.

We have already noted that the Poisson limit is obtained naturally for graphs which are subject to Dirichlet boundary conditions. The transition between the two extremes is affected by changing the parameter  $\Lambda_i = \lambda_i/v_i k$ . Using this time a fully

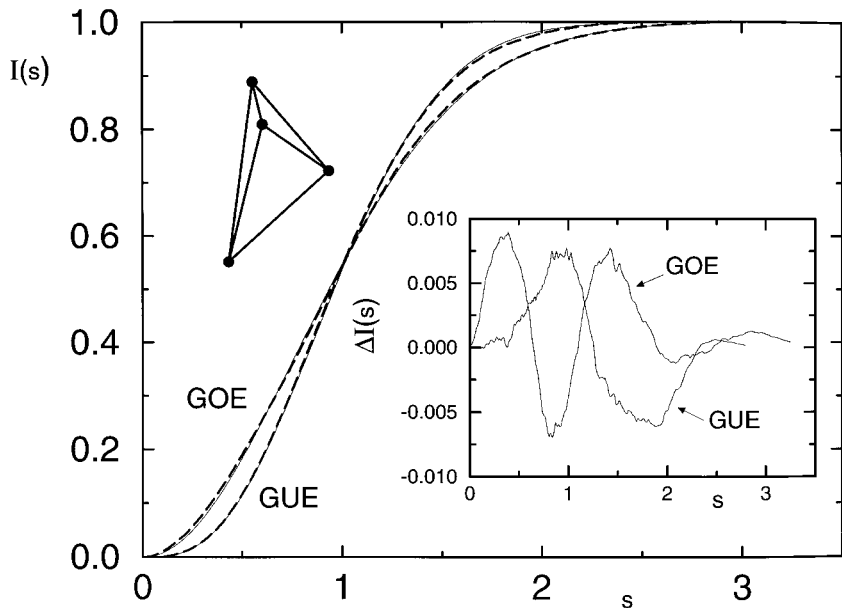


FIG. 4. Integrated nearest neighbor distribution  $I(s)$  for a fully connected quadrangle with  $A=0$  (Neumann boundary conditions). The results are based on the lowest 80,000 levels of a single realization of the bonds.  $\Delta I$  indicates the deviation from the exact GOE/GUE results.

connected pentagon, we observe the transition in the nearest neighbor distribution as is shown in Figs. 5a, 5b for  $A=0$  and  $A \neq 0$ , respectively.

We made similar comparisons for other well connected graphs and observed the same degree of agreement between the data and the results of RMT. Thus, we face an exceedingly simple class of systems which, according to the nearest neighbor statistics, belongs to the same spectral universality class as quantum systems which are chaotic in the classical limit. We shall study below other statistical measures and show that deviations from universality appear as expected and observed in generic Hamiltonian systems.

## 2. The Form Factor

To investigate further the dynamical origins of the level fluctuations we study the two point form factor  $K(\tau; k_0)$  defined by

$$K(\tau; k_0) = \frac{1}{\mathcal{N}} \left| \sum_{|k_n - k_0| \leq \Delta_k/2} e^{i2\pi k_n \mathcal{L} \tau} \right|^2 - \mathcal{N} \delta(\tau), \quad (74)$$

where we consider a spectral interval of size  $\Delta_k$ , centered about  $k_0$  and involving  $\mathcal{N} = \bar{d}\Delta_k$  eigenvalues.  $\tau$  measures lengths in units of the Heisenberg length  $l_H = \mathcal{L}$ . The main reason for our choice to base our analysis on the two point form factor

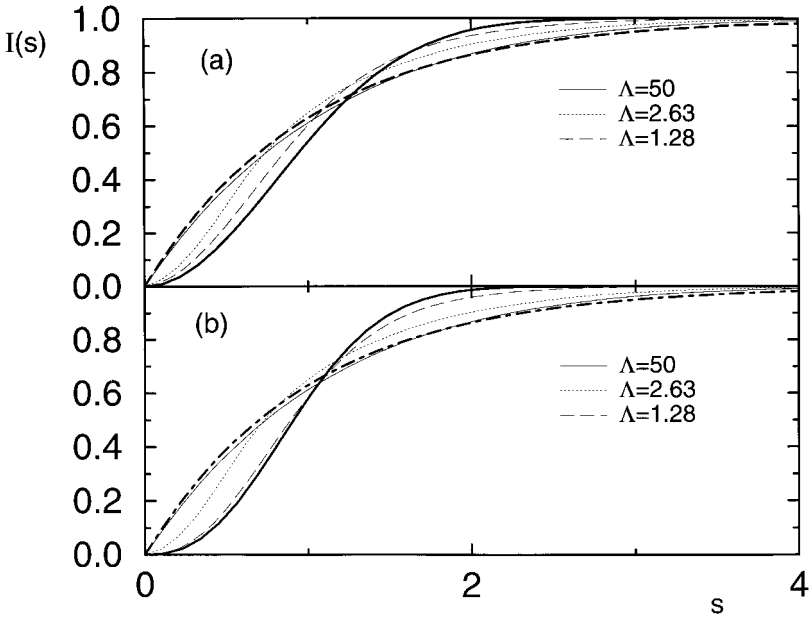


**FIG. 5.** The integrated nearest neighbor distribution  $I(s)$  for a fully connected pentagon and various values of the parameter  $\Lambda$ . The statistics was generated over a large number of realizations of the bonds of the graph; (a)  $A = 0$  and various values of the parameter  $\Lambda$ . (b)  $A \neq 0$  with the same boundary conditions as in (a). In both figures the thick solid line is the expectation of the corresponding RMT while the thick dashed line corresponds to Poisson.

is that it allows us to study the level fluctuations in terms of POs. Indeed, recalling that

$$\sum_{|k_n - k_0| < A_k/2} \exp(2\pi i k_n \mathcal{L} \tau) \equiv \int_{k_0 - A_k/2}^{k_0 + A_k/2} d(k) \exp(2\pi i k \mathcal{L} \tau) dk \quad (75)$$

and expressing  $d(k)$  by its PO expansion given by (35) we can rewrite  $K(\tau; k_0)$ , after substituting the resulting expression into (74), in terms of periodic orbits.

We shall concentrate for the time being on graphs with Neumann boundary conditions. Splitting  $K(\tau; k_0)$  to its diagonal  $K_D(\tau; k_0)$  and non-diagonal parts  $K_{ND}(\tau; k_0)$ , we write them in terms of periodic orbits and their repetitions

$$\begin{aligned} K_D(\tau; k_0) &= \frac{2\mathcal{N}}{\mathcal{L}^2} \sum_{p; r} |\mathcal{A}_p^r|^2 \left( \delta_{\mathcal{N}} \left( \frac{r l_p}{\mathcal{L}} - \tau \right) \right)^2 \\ K_{ND}(\tau; k_0) &= \frac{2\mathcal{N}}{\mathcal{L}^2} \sum_{p, r \neq p', r'} \mathcal{A}_p^r \mathcal{A}_{p'}^{r'} e^{i\pi(r\mu_p - r'\mu_{p'})} e^{iA(rb_p - r'b_{p'})} \\ &\quad \times \delta_{\mathcal{N}} \left( \frac{r l_p}{\mathcal{L}} - \tau \right) \delta_{\mathcal{N}} \left( \frac{r' l_{p'}}{\mathcal{L}} - \tau \right) \cos k_0(r l_p - r' l_{p'}), \end{aligned} \quad (76)$$

where we use  $\tilde{\mathcal{A}}_p = n_p l_p \mathcal{A}_p$  and  $\delta_{\mathcal{N}}(x) = (\sin(\mathcal{N}x/2))/(\mathcal{N}x/2)$ .  $K_D$  is a classical expression, because all interference effects are neglected, but for the ones which are due to exact symmetries. The sum-rule (48) enables us to justify a Hannay and Ozorio De Almeida-like sum rule [42], namely,  $K_D(\tau) \approx \langle g \rangle \tau$  [43] ( $\langle g \rangle$  is the mean degeneracy of the length spectrum due to exact symmetries such as time reversal). For  $\tau \ll 1$ ,  $K(\tau) \approx K_D(\tau)$ . Because of the fact that the quantum spectrum is real and discrete,  $K(\tau)$  must approach 1 for  $\tau > 1$ . This is taken care of by  $K_{ND}$ . In contrast to the diagonal part,  $K_{ND}$  depends crucially on the phase correlations between the contributing terms. Actually, its Fourier transform tests how the  $l_p$  spectrum is correlated [39]. In Hamiltonian systems in more than one dimension, the size of the spectral interval  $\Delta_k$  is limited by the requirement that the smooth spectral density is approximately constant. Here  $\bar{d}$  is constant, hence one can take arbitrarily large  $\Delta_k$ . This way, one can reach the domain where the function  $K(\tau)$  is composed of arbitrarily sharp spikes ( $\delta_{\mathcal{N}}(x)$  can become arbitrarily narrow) which resolve completely the length spectrum for lengths which are both smaller and larger than  $l_H$ . In Fig. 6a (Fig. 6b) we show the numerical  $K(\tau)$  calculated with two extreme values of  $\mathcal{N}$  for the case with (without) time reversal invariant symmetry. As long as  $\tau \mathcal{L}$  is shorter than the length of the shortest periodic orbit,  $K(\tau) = 0$ , while for  $\tau > 1$  it saturates and fluctuates around the value one. The RMT two-point form factor given as [33]

$$K_{\text{GOE}}(\tau) = \left\{ \begin{array}{ll} 2\tau - \tau \ln(1 + 2\tau), & 0 \leq \tau \leq 1 \\ 2 - \tau \ln\left(\frac{2\tau + 1}{2\tau - 1}\right), & \tau \geq 1 \end{array} \right\} \quad (77)$$

$$K_{\text{GUE}}(\tau) = \left\{ \begin{array}{ll} \tau, & 0 \leq \tau \leq 1 \\ 1, & \tau \geq 1 \end{array} \right.$$

is also shown in Figs. 6a and 6b for comparison. Despite the fluctuations, the low resolution curve does not deviate much from the prediction of RMT. The high resolution data shows a similar behavior, which can be better checked if one studies the integrated form factor (see inset of Figs. 6a, 6b)

$$\tilde{K}(\tau) = \frac{1}{\tau} \int_0^\tau K(t) dt. \quad (78)$$

However, by increasing the resolution, correlations between periodic orbits with different lengths are suppressed, and the interference mechanism which builds up  $K_{ND}$  cannot be due to the correlations in the spectrum of periodic orbit lengths, but to another source: For  $\tau > 1/2$  the periodic orbits must traverse some bonds more than twice. The likelihood of periodic orbits which traverse the same bonds the same number of times but with different back-scatter indices  $\mu_p$  is increasing, and the interferences which build  $K_{ND}$  are due to the sign correlations among orbits of exactly the same lengths (when  $A \neq 0$  one has to restrict the discussion to POs with the same *directed* length). This result demonstrates one important feature of the

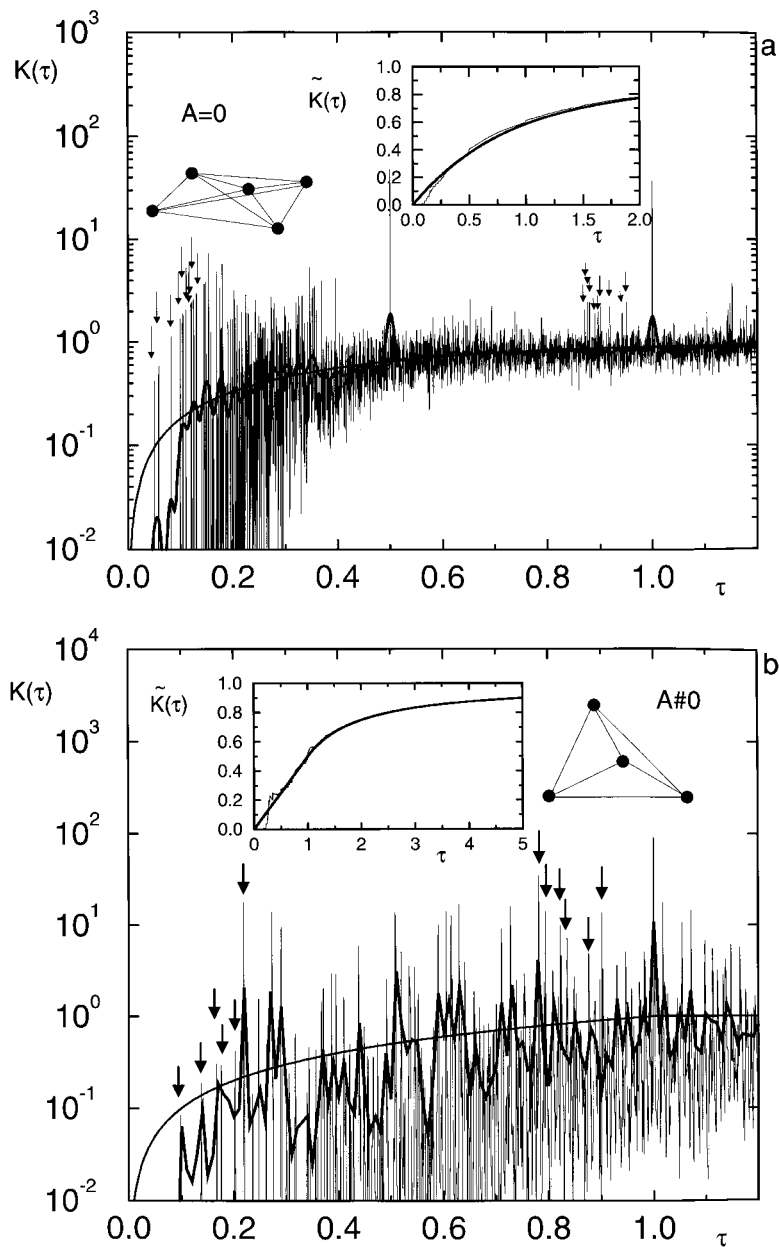


**FIG. 6.** Two point form factor ( $\approx 100,000$  levels). The arrows indicate the location of the short periodic orbits and their reciprocal lengths with respect to the Heisenberg length. In the insets we show the corresponding integrated form factor  $\tilde{K}(\tau)$  (thin line). (a) Fully connected pentagon with  $A=0$ ; (b) Fully connected quadrangle and  $A \neq 0$ . In both figures the bold lines are the expectation of the corresponding RMT.

periodic orbits correlations, namely, that periodic orbits carry not only metric information (lengths of trajectories) but also *topological information* (Maslov indices and degeneracies). The distribution of back scatter indices of periodic orbits is a problem that was not yet addressed by probabilistic graph theory. Our numerical results together with the general experience from quantum chaos allow us to conjecture that the spectral form factor connects RMT with the distribution of back scatter indices on POs.

Finally, the structure observed in the function  $K(\tau)$  decorating the rather smooth background can be attributed at low  $\tau$  to the short and rather scarce PO. The arrows in Figs. 6a, 6b indicate their location. The structures near  $\tau=1$  reproduce a trend which was predicted on different grounds in [36], namely, the spikes appear at lengths  $\mathcal{L} - l_p$  (see arrows in Figs. 6a, 6b). We can explain this phenomenon with the help of Newton's identities which relate  $\text{tr}(S(k))^n$  to the coefficients of the characteristic polynomial and the inversive symmetry of the latter (see (38)–(42)). Simple algebra gives

$$\sum_{n=1}^B \frac{\text{tr} S^{2B-n}}{2B-n} = e^{i\mathcal{L}k + \phi_0} \sum_{n=1}^B \frac{(\text{tr} S^n)^*}{n} + \dots, \quad (79)$$

where the phase  $\phi_0$  is independent of  $k$  and  $\dots$  stands for terms which involve amplitudes and phases of composite orbits. Substituting (32) and taking the

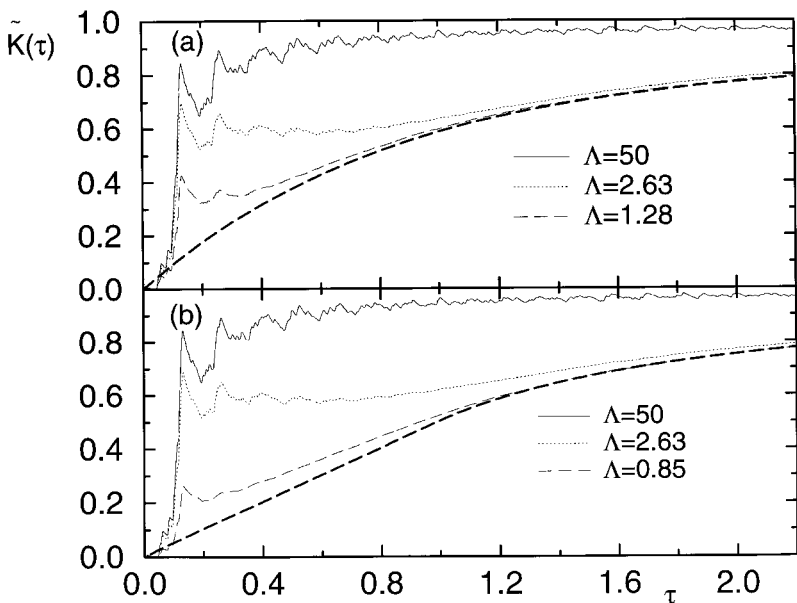


**FIG. 7.** The integrated two-point form factor  $\tilde{K}(\tau)$  for a fully connected pentagon. The thick dashed lines correspond to the RMT expectations. (a)  $A=0$  and various values of  $\Lambda$ . (b)  $A \neq 0$  and various values of  $\Lambda$ .

Fourier transform, we find that the contributions of the terms  $\text{tr } S^{2B-n}$  to the length spectrum appear at lengths  $\mathcal{L} - l_p$  where  $l_p$  are lengths associated with the shorter periodic orbits with periods  $n$ .

When graphs with mixed boundary conditions are investigated ( $\lambda \neq 0$ ), the parameter  $A$  which controls the spectral properties depends on the mean  $k_0$  parameter, and a transition from Poisson to RMT statistics is expected as  $k_0$  increases ( $A$  decreases). This transition is illustrated in Figs. 7a, 7b, where the dependence of  $\tilde{K}(\tau; k_0)$  on  $A$  is displayed.

### 3. Parametric Statistics

So far, we have shown that quantized graphs display most of the generic statistical properties encountered in the study of “quantum chaos.” We shall discuss now yet another statistics—the parametric statistics—and show that the analogy carries over also for this case. Parametric statistics are defined for systems which depend on an external parameter (to be denoted by  $\chi$ ), and they give a quantitative measure for the fluctuations due to level dynamics [44]. Among the first parametric properties studied were the velocity distribution  $\mathcal{P}(v)$  [45] (distribution of the first derivative of the levels), and the curvature distribution  $\mathcal{P}(c)$  (distribution of the second derivative of the levels) [46]. It has been shown that parametric statistics are universal for disordered or strongly chaotic systems provided the change of  $\chi$

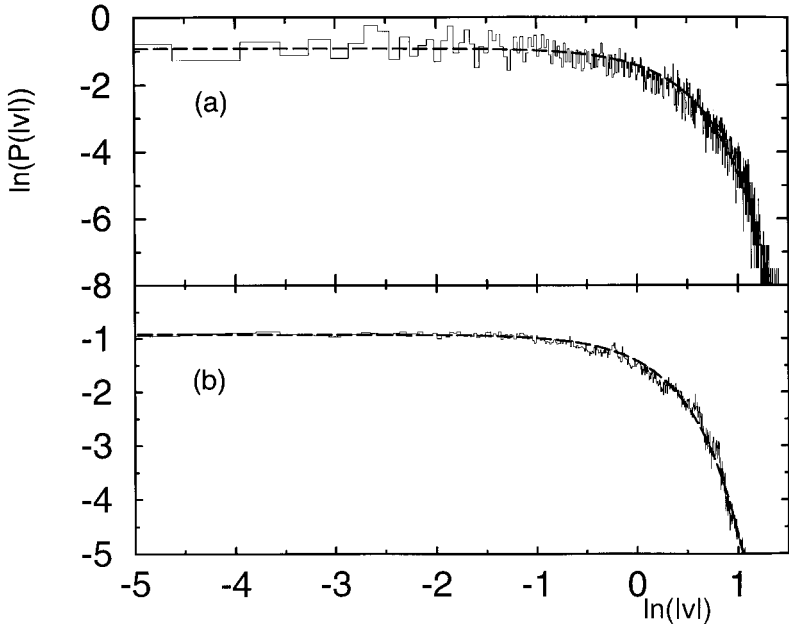


FIG. 8. Velocity distribution  $P(v)$  for a fully connected hexagon. The thick dashed line corresponds to a Gaussian with the same mean and standard deviation, with the numerical data; (a)  $A=0$ ,  $A_i=0$  (Neumann boundary conditions). (b)  $A \neq 0$ ,  $A_i=0$ .

does not modify global symmetries. As is usually the case, non-generic classical features may introduce deviations from the universal parametric statistics.

The parameter which was used to study level dynamics on the graphs was the bond length of an arbitrarily chosen pair of bonds,  $L_{i,j}(\chi) = L_{i,j}(0) - \chi$  and  $L_{i',j'}(\chi) = L_{i',j'}(0) + \chi$ , so that the total length  $\mathcal{L}$  is kept constant. In this way, the mean density  $\bar{d}$  is independent of  $\chi$ . Moreover, contrary to the usual studies of parametric statistics, the underlying classical dynamics of the graph are unaffected by the change of  $\chi$  (see also [47]). Modulating the two other parameters of our graphs, i.e., the “magnetic potential”  $A$  and the scattering potential  $\lambda$  at each vertex, we are able to study the parametric statistics in the transition regions where either time reversal symmetry or integrability are broken.

To reveal the universality in  $\mathcal{P}(v)$  and  $\mathcal{P}(c)$ , one uses the variance  $\sigma_v = \langle (\partial k_n / \partial \chi)^2 \rangle_k$  to rescale the velocities  $v$  and the curvatures  $c$

$$v_n = \frac{\partial k_n / \partial \chi}{\sqrt{\sigma_v}}, \quad c_n = \frac{1}{\beta\pi} \frac{\partial^2 k_n / \partial \chi^2}{\sigma_v}, \quad (80)$$

where  $\beta = 1, 2$  correspond to graphs with or without time reversal symmetry, respectively.

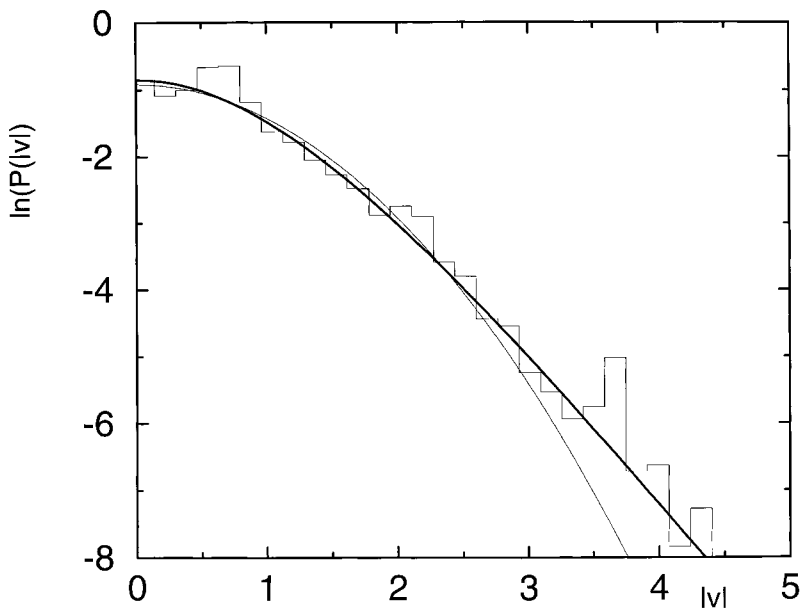
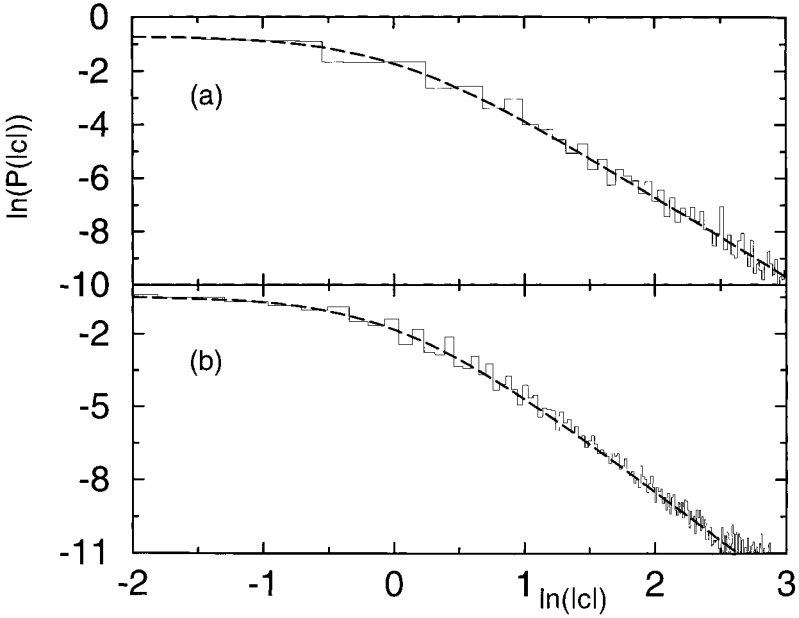


FIG. 9. Velocity distribution  $P(v)$  for a fully connected hexagon.  $A = 0$ , and  $A_i = A = 4.97$ . The thick solid line corresponds to (81) which describes the Poisson-GOE transition. The thin solid line corresponds to a Gaussian with the same mean and standard deviation, with the numerical data.



**FIG. 10.** Curvature distribution  $P(c)$  for the fully connected hexagon. The thick dashed line corresponds to (82) with  $\beta$  defined from the symmetry of the system. (a)  $A=0$  and  $A_i=0$  (Neumann boundary conditions). The parameter  $\beta=1$ . (b)  $A=20$  and  $A_i=0$ . The parameter  $\beta=2$ .

The numerical analysis reported below was conducted on a fully connected hexagon. For intermediate boundary conditions the wavenumber range, over which we performed our statistical analysis was kept small in order to keep the control parameter  $A$  to be essentially constant. Then the statistics was generated over realizations of the lengths of the bonds. By employing a finite-difference method, we were able to compute the level velocities and the curvatures for many different values of the parameter  $\chi$ . The total number of eigenvalues used to construct the histograms exceeded 186,000 in each statistic.

We first analyze the velocity distributions for graphs. For level dynamics within the GOE or the GUE the distribution of level velocities  $\mathcal{P}(v)$  is proved to be Gaussian [45]. Some of our results are shown in Fig. 8a, 8b, for  $A=0$  and  $A \neq 0$ , respectively (in both cases, Neumann boundary conditions were imposed). The calculated velocity distributions are well approximated by a Gaussian of the same mean value and standard deviation.

Fyodorov [48] derived an analytical formula for  $\mathcal{P}(v)$  which applies for disordered systems in the strongly localized limit and for which time reversal symmetry is violated

$$\mathcal{P}(v) = \frac{\pi}{6} \frac{\pi v \coth(\pi v/\sqrt{6}) - \sqrt{6}}{\sinh^2(\pi v/\sqrt{6})}. \quad (81)$$

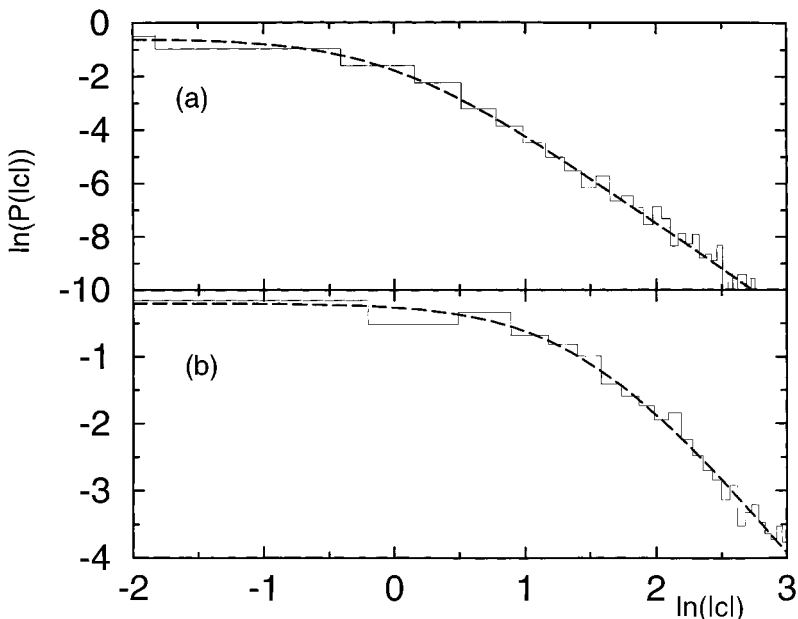


**FIG. 11.** Curvature distribution  $P(c)$  for the fully connected hexagon. The thick dashed line corresponds to (82) with  $\beta$  defined from the symmetry of the system (fitting parameter). (a)  $A = 2$  and  $A_i = 0$ . The fitting parameter is  $\beta = 1.4 \pm 0.1$ ; (b)  $A = 0$  and  $A_i = A = 4.97$ . The statistics were generated as explained in the text. The fitting parameter is  $\beta = 0.28 \pm 0.01$ .

Numerical simulations have shown that this formula is also applicable in the domain where the Poisson-GOE transition takes place [47]. Our numerical results, presented in Fig. 9, show that (81) reproduce the data in the range of large  $A$  values, thus confirming the suggestion first made in [47].

RMT predicts explicit expressions for the curvature distributions  $\mathcal{P}(c)$  [46, 48]

$$\mathcal{P}(c) = N_\beta \frac{1}{(1 + c^2)^{(\beta+2)/2}}, \quad (82)$$

where  $N_\beta$  equals 0.5 and  $2/\pi$  for GOE ( $\beta = 1$ ) and GUE ( $\beta = 2$ ), respectively. Our numerical calculations for the cases with Neumann boundary conditions, and  $A = 0$ ,  $A \neq 0$  are shown in Figs. 10a, 10b respectively. The agreement with the theoretical expectation (82) is excellent.

In Ref. [47], it was suggested that (82) can be generalized for the intermediate statistics interpolating between Poisson and GOE or GUE. The normalization constant  $N_\beta$  has to be defined as

$$N_\beta = \frac{1}{\sqrt{\pi}} \frac{\Gamma((\beta+2)/2)}{\Gamma((\beta+1)/2)}. \quad (83)$$

and  $\beta$  takes real values within the interval  $(0, 2]$  (see [49]). We checked this conjecture for our system and we found that it describes in a satisfactory way the intermediate statistics. For this, we fitted the tails of the distribution of the second derivative of the levels (unscaled curvatures) to an algebraic decay  $\mathcal{P}(C) \sim C^{-(\beta+2)}$ . Then the value of  $\beta$  found from the fit was used in (80) to rescale the curvatures. Our results for the case of partially broken time reversal symmetry with  $A=2$  are shown in Fig. 11a. Similarly, in Fig. 11b we report our findings for the transition between Poisson and GOE.

## VI. GRAPHS WITH NON-UNIFORM CONNECTIVITY

So far, we have studied properties of well connected graphs and have shown that when the appropriate limit is taken, many statistical properties of the spectrum reproduce the expectations of RMT. We shall dedicate the next section to demonstrating cases for which the connectivity of the graph induces non uniform dynamics which has substantial effects on the corresponding quantum spectra and their statistics.

### A. The Hydra

As a first example of a family of graphs which is not uniformly connected, we studied the ‘‘Hydras’’ or ‘‘star’’ graphs. They are graphs which consist of  $v_0$  bonds, all of which emanate from a single common vertex labeled with the index  $i=0$ . The vertex at  $i=0$  will be referred to in the sequel as the Hydra’s *head*. The total number of vertices for such a graph is  $V=v_0+1$ , and the vertices at the end of the bonds will be labeled by  $i=1, \dots, V$ . We shall assume Neumann boundary conditions on these vertices. The Hydra is a bipartite graph, a property which implies, e.g., that there exist no periodic orbits of odd period! This is responsible for most of the non generic properties of the classical and the quantum properties of Hydras.

We start with the  $S_B$ -matrix statistics which will allow us a better physical understanding of our system. To this end we first calculate the matrix  $T$  defined in (17). One can easily show that

$$T = \begin{pmatrix} 0 & I \\ \sigma^{(0)} & 0 \end{pmatrix}. \quad (84)$$

The matrix  $\sigma^{(0)}$  is the  $v_0 \times v_0$  scattering matrix at the Hydra’s head as defined in (11).  $I$  denotes the  $v_0 \times v_0$  identity matrix. It represents the trivial back scattering at the vertices  $i=1, \dots, V$ . The  $S_B(k; A)$  matrix and its square  $S_B^2(k; A)$  can be written as

$$\begin{aligned}
S_B(k; A) &= \begin{pmatrix} 0 & d^{(+)} \\ d^{(-)}\sigma^{(0)} & 0 \end{pmatrix}; \\
S_B^2(k; A) &= \begin{pmatrix} d^{(+)}d^{(-)}\sigma^{(0)} & 0 \\ 0 & d^{(-)}\sigma^{(0)}d^{(+)} \end{pmatrix},
\end{aligned} \tag{85}$$

where  $d_{i,j}^{(\pm)} = \delta_{i,j} e^{i(k \pm A)L_j}$  are the diagonal matrices which carry the metric information. It follows from (85) that  $\text{tr} S_B^{2n+1} = 0$ , and the even traces satisfy  $\text{tr} S_B^{2n} = 2 \text{tr} S_H^n$ , where  $S_H \equiv d^{(-)}\sigma^{(0)}d^{(+)}$ .  $S_H$  is a  $v_0 \times v_0$  scattering matrix in the space of the Hydra bonds. It incorporates the reflections from the vertices  $i=1, \dots, V$ .  $S_H$  is independent of  $A$  since all the POs on the Hydra are self tracing, and from now on we shall study its properties, since it is free from the trivial effects which originate from the bipartite nature of the Hydra.

If we consider the limit  $v_0 \gg 1$ , then for  $n < v_0$ , we can use the diagonal approximation to calculate the form factor of the  $S_H$  matrix eigenphase spectrum. In the present context, the classical evolution operator which corresponds to the quantum  $S_H$  matrix is

$$(U_H)_{i,j} = \frac{2}{v_0^2} (1 + \cos \omega_0) + \left(1 - \frac{2}{v_0} (1 + \cos \omega_0)\right) \delta_{i,j}. \tag{86}$$

The spectrum of  $U_H$  consists of the values 1 and  $1 - 2((1 + \cos \omega_0)/v_0)$  which is  $v_0 - 1$  times degenerate. Therefore,

$$u_n \equiv \text{tr} U_H^n = 1 + (v_0 - 1) \left(1 - \frac{2}{v_0} (1 + \cos \omega_0)\right)^n. \tag{87}$$

For large valencies  $v_0$  the  $\text{tr} S_H^n$  are dominated by the  $n$  repetitions of fixed points. Thus, we can write for the trace of  $S_H^n$

$$\text{tr} S_H^n = \sum_{j=1}^{v_0} e^{2ikL_j n} \left(\frac{1 + e^{-i\omega_0}}{v_0} - 1\right)^n + \sum_p n_p g_p \mathcal{A}_p^r e^{iL_p k}, \tag{88}$$

where the second sum contains contributions from other periodic orbits. By performing furthermore an average over realizations of the lengths of the bonds of Hydras we get

$$\begin{aligned}
\langle |\text{tr} S_H^n|^2 \rangle &= v_0 \left| \left(\frac{1 + e^{-i\omega_0}}{v_0} - 1\right)^n \right|^2 \\
&+ n \left[ u^n - v_0 \left(\frac{2}{v^2} (1 + \cos \omega_0) - \frac{2}{v_0} (1 + \cos \omega_0) + 1\right)^n \right].
\end{aligned} \tag{89}$$

In the second term of the r.h.s. of (89) we have subtracted from the classical return probabilities  $u_n$  (see (87), the contributions from the fixed points which already had been taken into account). Equation (89) can be written in a better form, i.e.,

$$\begin{aligned} \frac{1}{v_0} \langle |\text{tr } S_H^n|^2 \rangle &= \left[ \frac{2(1-v_0)(1+\cos \omega_0) + v_0^2}{v_0^2} \right]^n \\ &+ \frac{n}{v_0} \left[ (v_0-1) \left( 1 - 2 \frac{1+\cos \omega_0}{v_0} \right)^n + 1 \right] \\ &- n \left[ \frac{2}{v_0^2} (1+\cos \omega_0) - \frac{2}{v_0} (1+\cos \omega_0) + 1 \right]^n. \end{aligned} \quad (90)$$

This is different from the generic expression in two important ways: The linear term which dominates the larger  $n$  domain is proportional to  $n$  and not to  $2n$  because in the Hydra all the periodic orbits are self tracing. The other two terms which dominate the domain of smaller  $n$  are due to the  $n$  repetitions of fixed points and to small (degenerate) eigenvalues of  $U_H$ . Their  $n$  dependence cannot be scaled with  $v_0$ , and they represent a typical transient effect. The spectrum of  $S_H$  is not degenerate, and therefore for  $n > v_0$  the form factor reaches its asymptotic value 1. This transition is due to the interference of contributions of periodic orbits with the same lengths, but even for the simple Hydra graphs we do not have a theory which explains this phenomenon.

The above approximation applies quite well also for the Dirichlet boundary conditions. Indeed, for  $\omega_0 = \pi$  we have from (90) that  $(1/v_0) \langle |\text{tr } S_H^n|^2 \rangle = 1$ . Moreover, the transition to the Poisson limit is again described quite well by (90), for  $\tau \equiv n/v_0 < 1$ . This is shown in Fig. 12 for a Hydra with  $v_0 = 50$  and various values of the parameter  $A_0$ . The non generic features expected from the periodic orbit theory are well reproduced by the numerical data.

The wavenumber spectrum follows the same trends as the eigenphase spectrum discussed above. The secular Eq. (5) for Hydras takes a particularly simple form,

$$\sum_{j=1}^{v_0} \tan kL_j = \frac{\lambda_0}{k}. \quad (91)$$

Here, we investigate for simplicity the case of Hydras with a zero scattering potential  $\lambda_0 = 0$ . In Fig. 13 we present the level spacing distribution  $P(s)$  for various valencies. In all cases, the spectrum shows level repulsion, which is described rather well by the Wigner surmise for large valencies. A closer look shows deviations which do not decrease when the valency increases. In particular, in the limit  $s \rightarrow 0$ , the  $I(s)$  does not approach the expected power law, and this can be seen in the inset of Fig. 13 where the results for Hydras with  $v_0 = 7 - 18$  are compared with the GOE expression. In light of the discussion of the  $S_H$  eigenvalues statistics, the deviations observed in the nearest neighbor spacings distribution are not surprising.

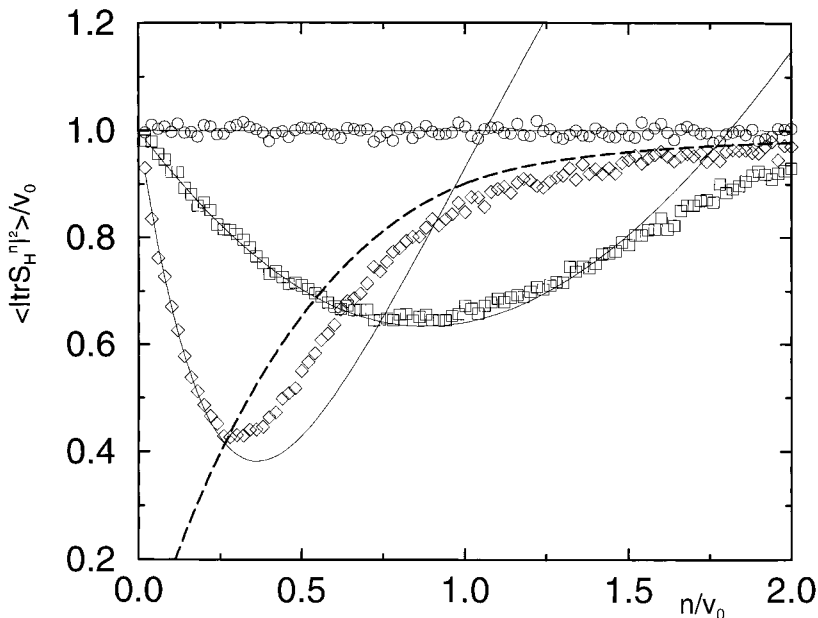


FIG. 12. The phase-shift form factor for a Hydra with  $v_0 = 50$  and  $A_0 = 2000$  ( $\circ$ ),  $A_0 = 2$  ( $\square$ ), and  $A_0 = 0$  ( $\diamond$ ). The thin solid lines correspond to the theoretical expectation (90), while the thick dashed line to the RMT prediction.

In a previous publication [23] we investigated the two point form factor  $K(\tau)$  for the Hydras and we had reported (for the case  $v_0 = 5$ ) quite good agreement with RMT predictions. However, upon increasing  $v_0$ ,  $K(\tau)$  shows the same behavior as its counterpart for the eigenphase spectrum of  $S_H$ . In Fig. 14 we present the two-point form factor for Hydras with  $v_0 = 5, 15$ . The deviations from RMT predictions, as we are increasing the valency, follow the pattern observed for the  $S_H$  spectral statistics (see (90)).

As expected, the Hydra spectrum displays non generic spectral statistics, which reflect the special connectivity and hence the classical dynamics of this graph. Periodic orbits theory (in particular, its diagonal approximation) reproduces the statistics which relate to the limit of short evolution times.

### B. Rings With Variable Connectivity

In this section we shall study a family of regular graphs which are defined by the connectivity matrix

$$C_{i,j} = \begin{cases} 1 & \text{for } i \neq j \text{ and } |i-j| \leq b \\ 0 & \text{for } i = j \text{ or } |i-j| > b \end{cases} \quad (92)$$

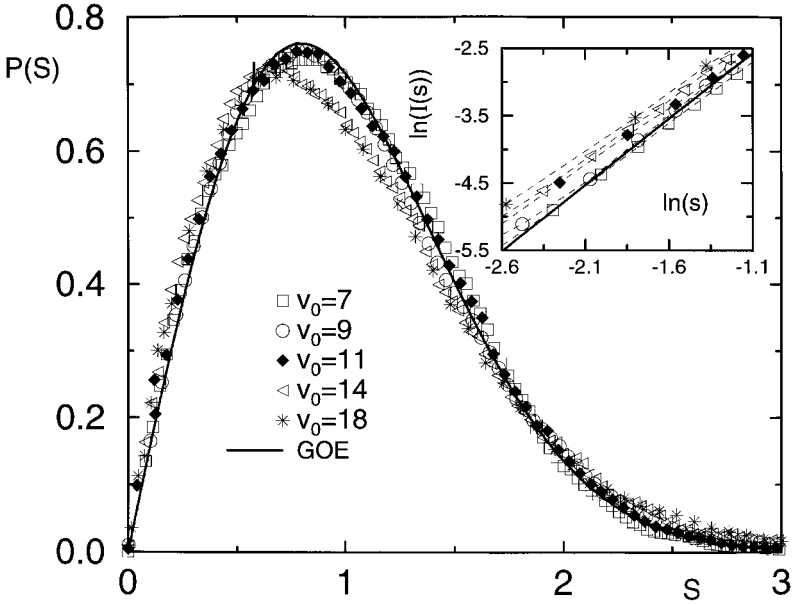


**FIG. 13.** Nearest level spacing distribution  $P(s)$  for various valencies  $v_0$  of the Hydras and  $\lambda_0=0$ . In the inset we report the integrated level spacing  $I(s)$  vs  $s$ , for small spacings (the dashed lines are guides for the eye). Deviations from RMT (thick solid line) are clearly observed.

so that  $2b$  is the valency. When the graph is drawn in the plane, with the  $V$  vertices placed on a circle with  $\theta_i > \theta_j$  for  $i > j$ , and  $V \gg b$ , then the resulting shape is a ring, and hence the name.

We shall study the spectral statistics as a function of the valency and will attempt to answer the question: At what value of  $b$  can we consider the graph as sufficiently well connected so that its spectral properties can be reproduced by RMT? We shall assume Neumann boundary conditions throughout this section.

As long as  $1 < b \ll V$ , the classical evolution operator describes a random walker on a ring, where the hopping step size can take any value between 1 and  $b$ . This results in a diffusive evolution on the ring, with  $D \approx \frac{2}{3}\pi^2 b^2$ . The case  $b=1$  is trivial because the Neumann boundary conditions in this case do not allow reflections at the vertices, and hence, the particle goes around the ring “ballistically.” To eliminate this effect we added loops at each vertex. This does not alter the diffusive dynamics, but allows us to include rings with nearest neighbor hopping.

The quantum dynamics is strongly affected by the fact that the lengths of the bonds are rationally independent. In the limit  $b \ll V$  this causes the eigenstates to be localized, and the spectral correlations will bear the marks of the degree of localization. Our purpose is to study the transition in the spectral statistics of rings, as  $b$  is increased. The addition of loops to the vertices introduces also a subspace of eigenfunctions for which the vertex values  $\varphi_i=0$ , and the wavefunction itself

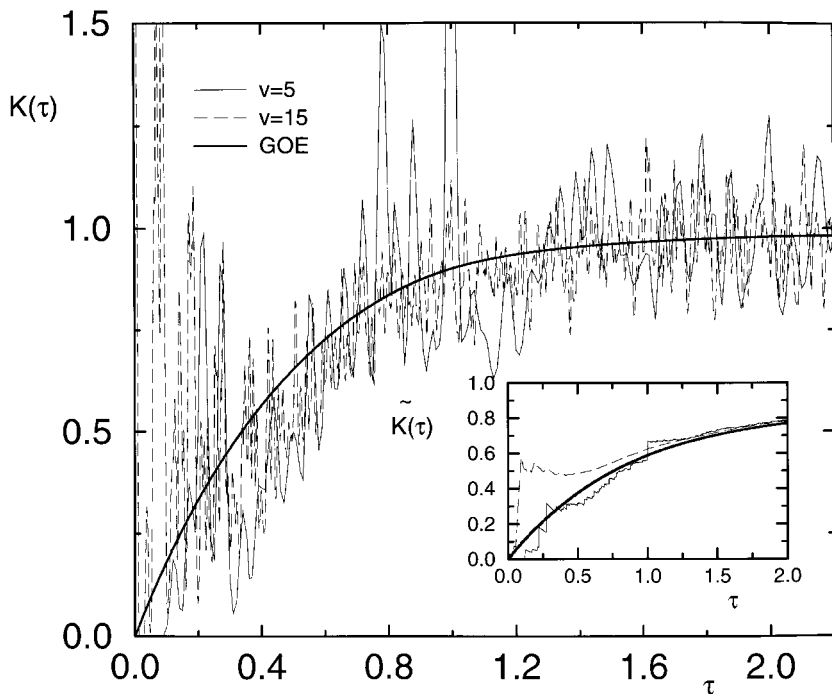


**FIG. 14.** The two-point form factor  $K(\tau)$  for Hydras with  $v_0=5$  (thin solid line) and  $v_0=15$  (thin dashed line). The thick solid line corresponds to the RMT expectations. In the inset we show the integrated form factor  $\tilde{K}(\tau)$ .

vanishes on all the bonds and all the loops but one. There it takes the form  $\sin(\pi n x / L_i^{(l)})$ , where  $L_i^{(l)}$  is the length of the loop attached at the  $i$  vertex. This subspace of eigenstates and the corresponding spectrum will be excluded from the following statistical study.

Starting with rings with  $b=1$ , we can calculate their properties by introducing the quantum transfer operator

$$T_N = \prod_{i=1}^V T_i; \quad (93)$$

$$T_i = \begin{pmatrix} 1 - \rho(k, A_i^{(l)}) & -\rho(k, A_i^{(l)}) \\ \rho(k, A_i^{(l)}) & 1 + \rho(k, A_i^{(l)}) \end{pmatrix} \cdot \begin{pmatrix} e^{i(k+A)L_i} & 0 \\ 0 & e^{i(-k+A)L_i} \end{pmatrix},$$

where the superscript  $(l)$  distinguishes the loops parameters. The bond  $(i-1, i)$  is referred to as the  $i$  bond. The parameter  $\rho$  is given by

$$\rho(k, A_i^{(l)}) = 2i \frac{\sin((A_i^{(l)} + k) L_i^{(l)}/2) \sin((A_i^{(l)} - k) L_i^{(l)}/2)}{\sin k L_i^{(l)}}. \quad (94)$$

By multiplying the transfer matrices for arbitrarily long segments, we calculated the Lyapunov exponent which yields the localization length  $l_\infty$ . Since for all  $k$  values we found it to be of order 1, we expect that the eigenfunctions for rings with  $V > 10$  will be well localized. A direct inspection of the eigenstates confirms this expectation (see Fig. 15).

The effect of localization on the spectral statistics can be understood by the following argument. As long as the total length  $\mathcal{L}$  of the ring is sufficiently larger than the Anderson localization length  $l_\infty$ , one can approximate the spectrum qualitatively as a union of  $\mathcal{L}/l_\infty$  uncorrelated spectra. One expects that the form factor for two rings with lengths  $\mathcal{L}$  and  $\mathcal{L}'$  will be related by [50]

$$K_{\mathcal{L}}(\tau) \simeq K_{\mathcal{L}'}(\tau \mathcal{L}/\mathcal{L}'). \tag{95}$$

In Fig. 16 we plot the integrated form factor  $\tilde{K}(\tau)$  (78) for  $b=1$  graphs with the number of vertices  $V=11$  and  $V=22$ . Scaling the  $\tau$  axis by 2, the two form factors coincide as expected. The relation (95) provides the correct sense in which one should interpret the statement that the spectrum of a localized system tends to the Poissonian limit as the size increases. The correlations in the spectrum remain, but they are on a scale which is  $\mathcal{L}/l_\infty$  larger than the mean spacing.

As the connectivity is increased, and keeping the length constant, one expects to see a transition in the spectral statistics. The first statistical quantity that we investigate is the integrated level spacing distribution  $I(s)$ . Our results for the case

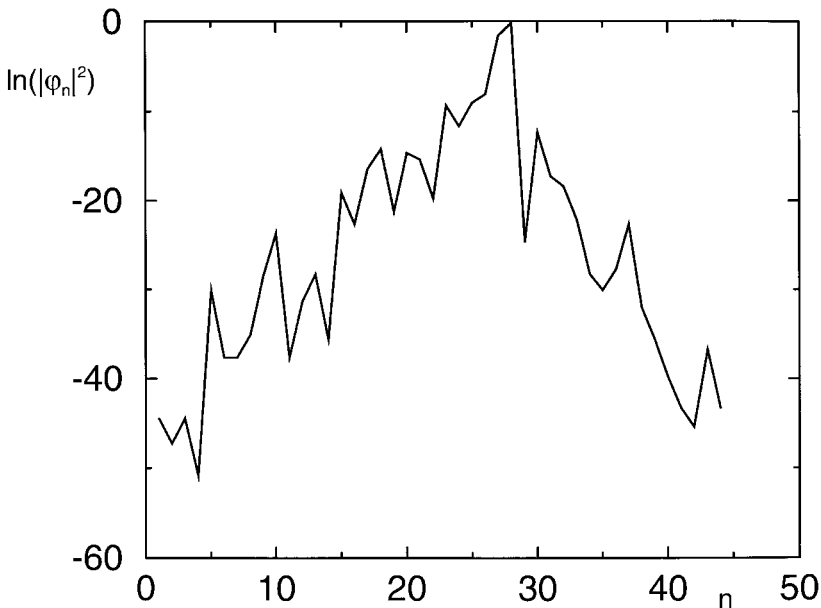


FIG. 15. A typical exponentially localized eigenstate of a graph with  $V=44$  and loops at each vertex.

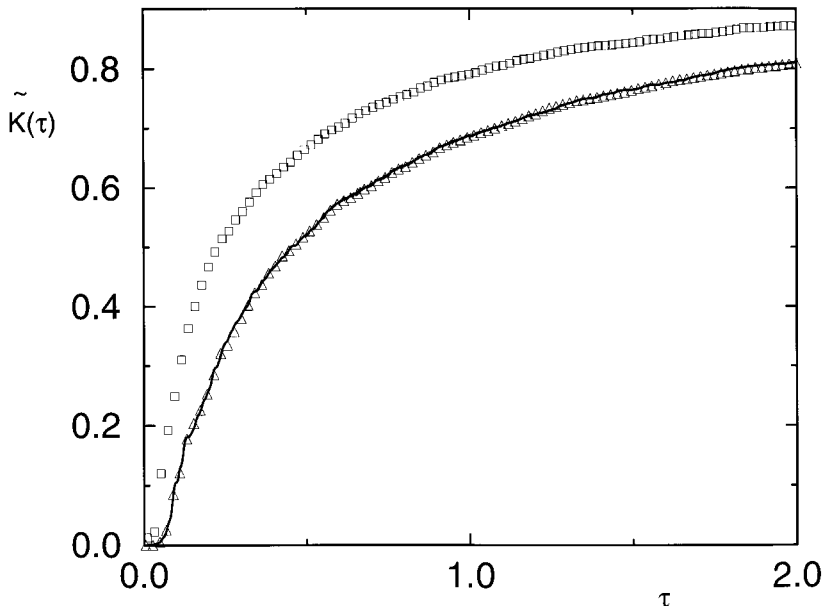


FIG. 16. The integrated form factor  $\tilde{K}(\tau)$  for graphs with  $V=11$  ( $\triangle$ ) and  $V=22$  ( $\square$ ) and loops at each vertex. The thick solid line corresponds to the graph with  $V=22$  after rescaling  $\tau$  by a factor of two.

$V=22$  are shown in Fig. 17. As the connectivity range increases,  $I(s)$  makes a transition from the Poisson distribution towards the GOE. Recently, it was suggested [51] that there exists a universal intermediate statistics, which applies for systems which undergo a transition from Poisson to RMT statistics. At the intermediate (critical) point,

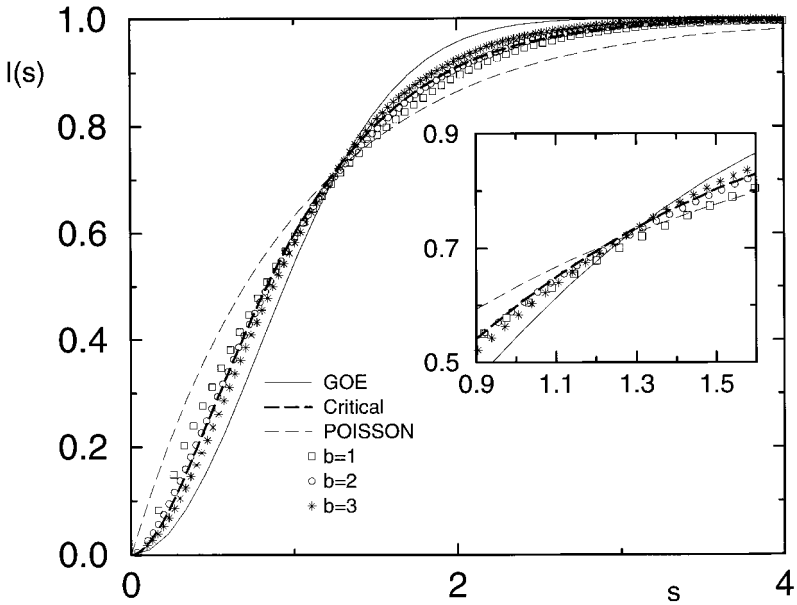
$$P_{cr}(s) = 4s \exp(-2s). \quad (96)$$

Figure 17 shows an excellent agreement between our numerical results for the ring with  $b=2$  and (96). A similar degree of agreement with the critical statistics appears also for other statistical measures like the number variance. The number variance  $\Sigma^2(L)$  probes the spectrum over all correlation lengths  $L$  and describes the fluctuations of the number  $n(L)$  of levels contained in a randomly chosen interval of length  $L$ . It is defined as

$$\Sigma^2(L) \equiv \langle (n(L) - L)^2 \rangle, \quad (97)$$

where the angular brackets  $\langle \rangle$  denote a local averaging over sufficiently many levels.  $\Sigma^2(L)$  is related with  $K(\tau)$  by the integral transform

$$\Sigma^2(L) = \frac{2}{\pi} \int_0^\infty d\tau \frac{\sin^2(\pi L\tau)}{\tau^2} K(\tau; \bar{k}). \quad (98)$$



**FIG. 17.** Integrated nearest neighbors distribution  $I(s)$  for a graph with loops at each vertex. The number of vertices is  $V=22$ . We consider various connectivities;  $b=1$  ( $\square$ ),  $b=2$  ( $\circ$ ),  $b=3$  ( $*$ ). The critical distribution (96) is also shown (thick dashed line) together with the GOE (thin solid line) and Poisson (thin dashed line) expressions.

and the reason that we chose here to concentrate on  $\Sigma^2(L)$  is that it behaves quite nicely, with respect to the highly fluctuative form factor.

The general expectation for generic systems [43] is that  $\Sigma^2(L)$  should comply with the predictions of RMT for small values of  $L$  (universal regime) and saturate to a non-universal value for large  $L$ 's due to the semiclassical contributions of short periodic orbits. Our results are presented in Fig. 18 together with the critical number variance which reads [51]

$$\Sigma_{cr}^2(L) = \frac{L}{2} + \frac{1 - \exp(-4L)}{8}. \tag{99}$$

For reference we also draw the number variance for a Poissonian spectrum given by  $\Sigma_2(L) = L$ , and the RMT expectation

$$\Sigma_2(L)_{\text{GOE}} = \frac{2}{\pi^2} \left\{ \ln(2\pi L) + \gamma + 1 + \frac{1}{2} \text{Si}^2(\pi L) - \frac{\pi}{2} \text{Si}(\pi L) - \cos(2\pi L) - \text{Ci}(2\pi L) + \pi^2 L \left( 1 - \frac{2}{\pi} \text{Si}(2\pi L) \right) \right\}, \tag{100}$$

where  $\gamma$  is the Euler constant.

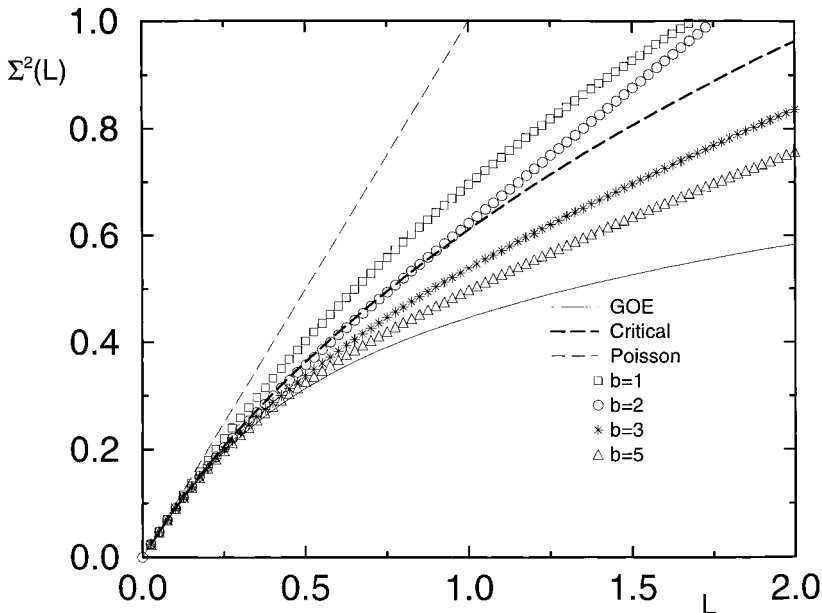


FIG. 18. The number variance  $\Sigma^2(L)$  for the graph of Fig. 17 and various connectivities;  $b=1$  ( $\square$ ),  $b=2$  ( $\circ$ ),  $b=3$  ( $*$ ),  $b=5$  ( $\triangle$ ). The critical distribution (99) is shown by the thick dashed line, together with the GOE (thin solid line) and Poisson (thin dashed line) results.

As one increases the connectivity the graph statistics approach the RMT expressions. On the basis of the estimate of the diffusion constant on the ring, we expect that the RMT limit is reached for  $b \simeq V$ .

## VII. CONCLUSIONS

The graph is a one-dimensional system. Yet, it is not simply connected, and this is why it can display chaotic classical dynamics, in the sense explained above. The fact that the graph is one dimensional can be seen in various classical and quantal attributes. On the quantum level, the smooth spectral counting function is proportional in general to  $E^{d/2}$  and indeed, in our case  $d=1$ . The stability factors in the trace formula correspond to a system with a single expanding direction, and no contracting direction. In this respect the graph trace formula is similar to the Riemann–Weyl trace formula. (The counting function for the Riemann zeros, however, has a logarithmic correction to the strictly one dimensional Weyl term.)

In spite of the simplicity of the graph Schroedinger operator, we have shown that the spectrum displays many features which appear in the study of the quantum analogues of classically chaotic systems. The limit  $\hbar \rightarrow \infty$  can be replaced by the limit  $\mathcal{L} \rightarrow \infty$ , which ensures that all the features which are due to the short and non generic periodic orbits are of lesser relative importance.

For a well connected graph, the length spectra of periodic orbits of periods larger than  $V$  show increasing degree of degeneracy as the period increases. These degeneracies give rise to the correct behavior of the form factor at large values of  $\tau$ . In other words, the fact that the quantum spectrum is real and discrete is expressed in the trace formula through the degeneracies of periodic orbit lengths and the distribution of the corresponding back-scattering indices. This observation points at a possible new interpretation of the Wigner–Dyson theory in terms of probabilistic graph theory.

The results reported here encourage us to believe that quantum graphs may serve as a convenient tool for the study of quantum chaotic or disordered systems. We do not know yet if it is possible to map any given Hamiltonian system onto a corresponding graph. The evidence is mounting, however, in favor of a very intimate link, and the search for this connection is one of our immediate goals.

### ACKNOWLEDGMENTS

This research was supported by the Minerva Center for Physics of Nonlinear Systems, and by a grant from the Israel Science Foundation. (T. K.) thanks the Feinberg School at the WIS for a Post Doctoral fellowship. We thank D. Cohen, D. Miller, H. Primack, Z. Rudnick and H. Schanz for valuable suggestions and comments, and Y. Colin De Verdiere for bringing J. P. Roth's paper [17] to our attention. In particular we thank U. Gavish for reading the manuscript critically and making valuable comments.

### REFERENCES

1. L. Pauling, *J. Chem. Phys.* **4** (1936), 673.
2. H. Kuhn, *Helv. Chim. Acta*, **31** (1948), 1441; H. Kuhn, *Helv. Chim. Acta*, **32** (1949), 2247.
3. J. R. Platt, *J. Chem. Phys.* **17** (1949), 484.
4. K. Rudenberg, *J. Chem. Phys.* **21** (1952), 1509; K. Rudenberg and C. W. Scherr, *J. Chem. Phys.* **21** (1953), 1565.
5. C. A. Coulson, *Proc. Phys. Soc. Lond.* **67** (1954), 608.
6. E. W. Montroll, *J. Math. Phys.* **11** (1970), 635.
7. Ph. Choquard, Lecture notes, *Phonon and Electrons II*, Section 3.1, 1971.
8. M. J. Richardson and N. L. Balazs, *Ann. Phys.* **73** (1972), 308.
9. S. Alexander, *Phys. Rev. B* **27** (1985), 1541.
10. C. Flesia, R. Johnston, and H. Kunz, *Europhys. Lett.* **3** (1987), 497.
11. R. Mitra and S. W. Lee, "Analytical Techniques in the Theory of Guided Waves," Macmillan, New York.
12. P. W. Anderson, *Phys. Rev. B* **23** (1981), 4828; B. Shapiro, *Phys. Rev. Lett.* **48** (1982), 823.
13. J. T. Chalker and P. D. Coddington, *J. Phys. C* **21** (1988), 2665; R. Klesse and M. Metzler, *Phys. Rev. Lett.* **79** (1997), 721; R. Klesse, Ph. D. Thesis, Universität zu Köln, AWOS-Verlag, Erfurt, 1996.
14. Y. Avishai and J. M. Luck, *Phys. Rev. B* **45** (1992), 1074; T. Nakayama, K. Yakubo, and R. L. Orbach, *Rev. Mod. Phys.* **66** (1994), 381.
15. Y. Imry, "Introduction to Mesoscopic Systems," Oxford, New York, 1996; D. Kowal, U. Sivan, O. Entin-Wohlman, Y. Imry, *Phys. Rev. B* **42** (1990), 9009.
16. J. E. Avron, in "Proc. 1994 Les Houches Summer School on Mesoscopic Quantum Physics" (E. Akkermans *et al.*, Eds.), p. 741, North-Holland, Amsterdam, 1995.

17. J.-P. Roth, in "Lectures Notes in Mathematics: Theorie du Potentiel" (A. Dold and B. Eckmann, Eds.), p. 521, Springer-Verlag, New York/Berlin.
18. P. Exner and P. Seba, *Rep. Math. Phys.* **28** (1989), 7; P. Exner, *J. Phys. A Math. Gen.* **29** (1996), 87.
19. P. Exner and R. Gawlista, *Phys. Rev. B* **53** (1996), 7275; P. Exner, *Phys. Rev. Lett.* **74** (1995), 3503.
20. J. E. Avron, P. Exner, and Y. Last, *Phys. Rev. Lett.* **72** (1994), 896.
21. R. Carlson, *Trans. Amer. Math. Soc.*, in press; R. Carlson, *Electron. J. Differential Equations* **23** (1997), 1; R. Carlson, *Electron. J. Differential Equations* **6** (1998), 1.
22. V. Kostyrykin and R. Schrader, Kirchhoff's rule for quantum wire, preprint.
23. T. Kottos and U. Smilansky, *Phys. Rev. Lett.* **79** (1997), 4794.
24. M. G. Gutzwiller, in "Chaos in Classical and Quantum Mechanics," Interdisciplinary Applied Mathematics (F. John, Ed.), Vol. 1, Springer-Verlag, New York, 1990.
25. J. P. Keating, *Nonlinearity* **4** (1991), 309.
26. U. Smilansky, in "Proc. 1994 Les Houches Summer School on Mesoscopic Quantum Physics" (E. Akkermans *et al.*, Eds.), p. 373, North-Holland, Amsterdam, 1995.
27. J. Gratus, C. J. Lambert, S. J. Robinson, and R. W. Tucker, *J. Phys. A Math. Gen.* **27** (1994), 6881.
28. T. Kottos and U. Smilansky, in preparation.
29. A. Selberg, *J. Ind. Math. Soc.* **20** (1956), 47.
30. E. Doron and U. Smilansky, *Nonlinearity* **5** (1992), 1055.
31. J. Keating and M. V. Berry, *Proc. Royal Soc. Lond. A* **437** (1992), 151.
32. U. Smilansky, in "Proc. 1989 Les Houches Summer School on Chaos and Quantum Physics" (M.-J. Giannoni *et al.*, Eds.), p. 371, North-Holland, Amsterdam, 1991.
33. M. L. Mehta, "Random Matrices and the Statistical Theory of Energy Levels," Academic Press, New York, 1990; T. A. Brody, J. Flores, J. B. French, P. A. Mello, A. Pandey, and S. S. M. Wong, *Rev. Mod. Phys.* **53** (1981), 385.
34. R. Blumel and U. Smilansky, *Phys. Rev. Lett.* **60** (1988), 472; R. Blumel and U. Smilansky, *Phys. Rev. Lett.* **64** (1990), 241.
35. F. Haake, M. Kus, H.-J. Sommers, H. Schomerus, and K. Zyczowski, *J. Phys. A* **29** (1996), 3641.
36. E. B. Bogomolny and J. P. Keating, *Phys. Rev. Lett.* **77** (1996), 1472; O. Agam *et al.*, *Phys. Rev. Lett.* **75** (1995), 4389.
37. U. Smilansky, *Phys. D* **109** (1997), 1767.
38. U. Smilansky, in "Proc., Nato Advanced Study Institute, Supersymmetry and Trace Formulae, 1997" (I. Lerner, Eds.), Cambridge, in press.
39. N. Argaman, F. M. Dittes, E. Doron, S. P. Keating, A. Y. Kitaev, M. Sieber, and U. Smilansky, *Phys. Rev. Lett.* **71** (1993), 4326; D. Cohen, H. Primack, and U. Smilansky, *Ann. Physics* **264** (1998), 108.
40. S. Kettmann, D. Klakow, and U. Smilansky, *J. Phys. A Math. Gen.* **30** (1997), 3643.
41. B. Dietz and F. Haake, *Z. Phys. B* **80** (1990), 153.
42. J. H. Hannay and A. M. Ozorio De Almeida, *J. Phys. A Math. Gen.* **17** (1984), 3429.
43. M. V. Berry, *Proc. Royal Soc. Lond. A* **400** (1985), 229.
44. J. Goldberg, U. Smilansky, M. V. Berry, W. Schweizer, G. Wunner, and G. Zeller, *Nonlinearity* **4** (1991), 1.
45. B. D. Simons and B. L. Al'tshuler, *Phys. Rev. B* **48** (1993), 5422.
46. P. Gaspard, S. A. Rice, H. J. Mikeska, and K. Nakamura, *Phys. Rev. A* **42** (1990), 4015; J. Zakrzewski and D. Delande, *Phys. Rev. E* **47** (1993), 1650; F. von Oppen, *Phys. Rev. E* **51** (1995), 2647; F. von Oppen *Phys. Rev. Lett.* **73** (1994), 798.
47. P. Kunstman, K. Zyczowski, and J. Zakrzewski, *Phys. Rev. E* **55** (1997), 2446.
48. Y. V. Fyodorov, *Phys. Rev. Lett.* **73** (1994), 2688; Y. V. Fyodorov and H.-J. Sommers, *Phys. Rev. E* **51** (1995), R2719; Y. V. Fyodorov and H.-J. Sommers, *Z. Phys. B* **99** (1995), 123.
49. F. M. Izrailev, *Phys. Rep.* **129** (1990), 299.
50. A. Pandey, *Ann. Phys. (N.Y.)* **134** (1981), 110.
51. E. B. Bogomolny, in preparation.